



Hydrodynamic chromatography coupled to single-particle ICP-MS for the simultaneous characterization of AgNPs and determination of dissolved Ag in human plasma and blood of burnt patients.

Journal:	<i>Analytical and Bioanalytical Chemistry</i>
Manuscript ID:	ABC-01228-2015.R1
Type of Paper:	Research Paper
Date Submitted by the Author:	n/a
Complete List of Authors:	Roman, Marco; University Ca' Foscari of Venice, Environmental Sciences, Informatics and Statistics; CNR, Institute for the Dynamic of Environmental Processes Venice Rigo, Chiara; University Ca' Foscari of Venice, Environmental Sciences, Informatics and Statistics Castillo-Michel, Hiram; European Synchrotron Radiation Facility, Munivrana, Ivan; University School of Medicine, Clinic of Plastic and Reconstructive Surgery and Burn Centre Vindigni, Vincenzo; University School of Medicine, Clinic of Plastic and Reconstructive Surgery and Burn Centre Mičetić, Ivan; European Center for the Sustainable Impact of Nanotechnology, Benetti, Federico; European Center for the Sustainable Impact of Nanotechnology, Manodori, Laura; European Center for the Sustainable Impact of Nanotechnology, Cairns, Warren; CNR, Institute for the Dynamic of Environmental Processes
Keywords:	Silver nanoparticles, Hydrodynamic chromatography, Single-particle ICP-MS, Synchrotron radiation, Burns, Wound dressings

1
2
3 **Hydrodynamic chromatography coupled to single-particle ICP-MS for the simultaneous**
4 **characterization of AgNPs and determination of dissolved Ag in human plasma and blood of**
5 **burnt patients**
6
7

8
9 Marco Roman^{1,2*}, Chiara Rigo¹, Hiram Castillo-Michel³, Ivan Munivrana⁴, Vincenzo Vindigni⁴, Ivan
10 Mičetić⁵, Federico Benetti⁵, Laura Manodori⁵, Warren R.L. Cairns²
11

12 ¹ Ca' Foscari University of Venice, Department of Environmental Sciences, Informatics and
13 Statistics (DAIS), Dorsoduro 2137, 30123 Venice, Italy

14 ² Institute for the Dynamics of Environmental Processes (IDPA-CNR), Dorsoduro 2137, 30123
15 Venice, Italy

16 ³ European Synchrotron Radiation Facility (ESRF), 71 avenue des Martyrs, 38000 Grenoble, France

17 ⁴ Burns Center, Division of Plastic Surgery, University Hospital of Padua, Via Giustiniani 2, 35128
18 Padua, Italy

19 ⁵ European Center for the Sustainable Impact of Nanotechnology (ECSIN), Viale Porta Adige 45,
20 45100 Rovigo, Italy
21
22

23
24 Corresponding author: Marco Roman

25 Ca' Foscari University of Venice, Department of Environmental Sciences, Informatics and Statistics
26 (DAIS), Dorsoduro 2137, 30123 Venice, Italy

27 Phone: +0039 041 234 8545

28 Email: marco.roman@unive.it
29
30
31

32 **Abstract**

33 Silver nanoparticles (AgNPs) are increasingly used in medical devices as innovative antibacterial
34 agents, but no data are currently available on their chemical transformations and fate *in vivo* in
35 the human body, particularly on their potential to reach the circulatory system. To study the
36 processes involving AgNPs in human plasma and blood, we developed an analytical method based
37 on hydrodynamic chromatography (HDC) hyphenated to ICP-MS in single-particle detection mode.
38 An innovative algorithm was implemented to deconvolute the signals of dissolved Ag and AgNPs,
39 and to extrapolate a multiparametric characterization of the particles in the same chromatogram.
40 From a single injection, the method provides the concentration of dissolved Ag and the
41 distribution of AgNPs in terms of hydrodynamic diameter, mass-derived diameter, number and
42 mass concentration. This analytical approach is robust and suitable to study quantitatively the
43 dynamics and kinetics of AgNPs in complex biological fluids, included processes such as
44 agglomeration, dissolution, and formation of proteins coronas. The method was applied to study
45 the transformations of AgNPs standards and an AgNPs-coated dressing in human plasma,
46 supported by μ XRF and μ XANES speciation analysis and imaging, and to investigate for the first
47 time the possible presence of AgNPs in the blood of three burnt patients treated with the same
48 dressing. Together with our previous studies, the results strongly support the hypothesis that the
49 systemic mobilization of the metal after topical administration of AgNPs is driven by their
50 dissolution *in situ*.
51
52
53
54

55 **Keywords**

56 Silver nanoparticles; Hydrodynamic chromatography; Single-particle ICP-MS; Synchrotron
57 radiation; Burns; Wound dressings
58
59
60

Introduction

The multispectral antimicrobial effects of silver (Ag) are known and have been exploited since ancient times, but its use in consumer products and medical devices has proliferated considerably in recent years [1]. Ag-containing devices are widely used in hospitals as adjuvants in the treatment of pathologies where the control of bacterial infections is a key factor for a favourable prognosis [1,2]. The treatment of burns and chronic skin lesions is one of the most important applications because the local interruption of the blood flow make systemic infection prophylaxes little effective, and topical administration of Ag-based antimicrobials may therefore be decisive in preventing sepsis [2].

The reactivity of Ag in biological systems is mainly due to the ionic form Ag^+ , thanks to its ability to bind organic ligands [3]. In bacteria, such interactions allow the metal to bind to the cell wall, enter the cytoplasm, and interfere in key metabolic pathways [4]. However, the high reactivity of Ag^+ in biological systems may also lead to a rapid deactivation and clearance of the metal, mediated for example by complexation with serum proteins [5]. Engineered nanoparticles (NPs) provide innovative forms of Ag which can be specifically designed to modulate the release of ions from their surface in a gradual and highly controlled way [6]. Metallic AgNPs have the potential to persist sufficiently for mobilization within biological tissues, and exhibit enhanced affinity for cellular membranes, all of which favours their uptake and delivery to intracellular targets [7]. Several physico-chemical characteristics of AgNPs are determinant for their dynamics, including size/shape, surface charge and coating, as well as aggregation/agglomeration state. Many properties of the medium also affect their stability in biological systems, including the ionic strength, pH, pE, and composition of the organic matter [4]. Complex interactions among these properties of AgNPs and the surrounding media have been conjectured to regulate their transformations in environmental and biological systems [3], but the actual dynamics *in situ* and *in vivo* in human tissues remain currently unknown.

A key question is to establish whether AgNPs are able to remain intact for a sufficient length of time and space to reach the bloodstream and undergo systemic distribution. To address this question, adequate analytical tools to detect AgNPs and dissolved Ag in blood must be developed. Techniques such as transmission electron microscopy (TEM), scanning electron microscopy (SEM) and atomic force microscopy (AFM) enable size characterization of NPs at high resolution [8-10], but cannot provide statistically robust and quantitative data on complex biological fluids with a very low concentration of the metal. Dynamic and static light scattering (DLS and SLS) are widely used to characterize NPs suspensions, but are also inadequate for the analysis of polydisperse particles in complex biological matrices [11,12]. In addition, none of these techniques provides information on the dissolved fraction of a metal. A powerful technique for quantitative detection of metallic NPs is ICP-MS, as it is element-specific and highly sensitive, although it has to be coupled to a separation technique to gain a dimensional characterization. A variety of separation techniques, including flow-field-flow fractionation (FFF), hydrodynamic chromatography (HDC), reverse-phase (RP) high performance liquid chromatography (HPLC), ion mobility chromatography (IMC) and micellar electrokinetic chromatography (MEC), have been coupled to ICP-MS for the characterization of AgNPs in standard solutions, plasma and serum, nutraceuticals and a beverage [13-16,11,17,18]. However, all these separation techniques have limitations. Low recoveries are a critical issue in FFF, due to the complex interactions of AgNPs with the membrane, and dissolved ions cannot be detected [11]. RP-HPLC is able to separate AgNPs from ionic Ag, but with poor resolution and low reproducibility for complex biological matrices such as bovine serum [18]. HDC is a robust and versatile method for separating NPs even in complex and heavy matrices, but with poor resolving power. Dissolved ions could also be potentially determined by HDC-ICP-MS, but this

1
2
3 application has not yet been explored. MEC-ICP-MS could enable the size-dependent separation of
4 AgNPs and ionic Ag with a higher resolving power, but has only been tested on standards [19]. The
5 recent introduction of the single-particle (sp) acquisition mode in ICP-MS has allowed this
6 technique to detect NPs individually, providing quantitative information on their mass distribution
7 and number concentration in solutions [20]. A number of applications have been proposed for the
8 characterization of AgNPs in waters [21-25], but biological matrices remain virtually unexplored,
9 with the exception of enzymatically digested chicken meat [26]. However, spICP-MS does not
10 provide key data for the dynamics of AgNPs in complex systems, including the real diameter,
11 shape, composition, and aggregation/agglomeration of the particles, because only their metallic
12 mass can be revealed. The most promising strategy to obtain complete information on NPs in
13 complex media are spICP-MS hyphenated techniques, but only a few applications have been
14 proposed until now. Online coupling of asymmetric FFF (AF4) to spICP-MS has been explored to
15 study AgNPs in chicken meat [27], and so has HDC-spICP-MS for Ag, Au and polymeric NPs in
16 standards solutions and waters [28,16,12]. The determination of dissolved Ag in combination with
17 spICP-MS remains an analytical challenge. Off-line separation of the dissolved fraction by
18 ultrafiltration has been proposed [29,24], but simultaneous on-line methods would be preferable.
19 Statistical separation of the signals generated by AgNPs and dissolved Ag is possible in spICP-MS
20 by adopting a simple threshold value fixed on the standard deviation of the background
21 [12,25,21,30], or by applying a more complex algorithm based on polygaussian fitting of the
22 frequency distribution [31]. However, such strategies are not suitable for hyphenated techniques,
23 in which dissolved Ag itself generates a transient signal. Thus, the deconvolution of signals from
24 dissolved Ag and AgNPs in spICP-MS hyphenated techniques has not yet been attempted.
25 The goals of the present work were to set up and apply an analytical method based on HDC
26 hyphenated to spICP-MS for the simultaneous determination of dissolved Ag and the full
27 characterization of AgNPs in human plasma/blood based on an innovative signal deconvolution
28 strategy. An innovative approach combining our method with μ XRF imaging and μ XANES
29 speciation analysis was applied to study *in vitro* the transformations of AgNPs incubated in whole
30 human plasma, and to investigate for the first time the presence of AgNPs in the whole blood of
31 burnt patients treated by topical administration of AgNPs under real hospital conditions.
32
33
34
35
36
37
38

39 1. Experimental

40 Standards, reagents and samples

41 An Ag ICP-MS grade 1000 ng mL^{-1} standard solution (certificated, NIST teachable) was obtained
42 from Ultra Scientific (Bologna, Italy) and used to calibrate the total Ag measurements. Commercial
43 standards of AgNPs purchased from Sigma-Aldrich were used for method development,
44 calibrations and the incubation experiments. The standards consisted of monodisperse metallic
45 NPs with nominal diameters of 10, 20, 40, 60 and 100 nm (provided uncertainty $\pm 4 \text{ nm}$), mass
46 concentration $20 \pm 0.5 \mu\text{g mL}^{-1}$, suspended in aqueous solution and stabilized with sodium citrate.
47 The standards were characterized by TEM resulting in a size distribution compatible with the
48 values provided by the manufacturer, and spherical shape. The z-potential of the mother
49 dispersions was measured confirming their good stability ($< -40 \text{ mV}$). Details on the experimental
50 procedures for characterization of the standards, representative TEM images and a summary of
51 their size/shape parameters and z-potential can be found in the appendix. The measured size of
52 the standards was used for all calculations, but for simplicity, we refer to their nominal diameter
53 throughout this paper. The exact mass concentration as total Ag of the mother dispersions was
54 also measured by ICP-MS, and number concentration was calculated based on the experimental
55 mode of the size distribution.
56
57
58
59
60

1
2
3 The commercial dressing Acticoat Flex3™ (Smith & Nephew) was used for the *in vitro* incubations
4 and the *in vivo* treatment of burnt patients as reported elsewhere [32]. The mobile phase for
5 chromatography was prepared using sodium dodecyl sulphate (SDS), HNa_2PO_4 dihydrate and
6 IGEPAL® CA-630 nonionic detergent in the following concentrations: SDS 0.05 % v/v, HNa_2PO_4
7 0.002 M and IGEPAL 0.1 % v/v at pH 7.4. A water solution containing tetramethylammonium
8 hydroxide (TMAH) 0.1 % v/v, NH_4OH 2.8 % w/w and Triton™ X-100 0.1 % v/v was used to dilute
9 20-fold the whole blood for total Ag determination by ICP-MS. L-glutathione reduced (GSH) and
10 human serum albumin (HSA) lyophilized powders were used for incubation experiments. All
11 incubations were carried out in a normal laboratory environment at 37 °C in a thermostated bath,
12 under constant gentle shaking in the dark. The preparation steps for standards and samples were
13 carried out in a class 1000 clean room environment under a class 100 laminar flow bench.

14
15 Whole human plasma for incubations and control whole blood were provided by distinct
16 volunteers and were collected at the University Hospital of Padua. Four samples of whole blood
17 were provided by the bio-bank of the same Hospital, and were collected from three adult patients
18 treated in the same Hospital, at the Burns Center, following the current protocols without any
19 additional invasive procedure. The patients did not present any pathology other than the burn. All
20 samples were collected and stored in agreement with the guidelines of the University Hospital of
21 Padua and informed consent of the patients was obtained according to the Helsinki Declaration.
22 The blood was collected in purple-tip vials (K2-3EDTA) in order to prevent coagulation, was
23 immediately frozen to lyse the red blood cells, and was stored frozen until analysis.

24 Instrumentation

25
26 The chromatographic system consisted of an Agilent Technologies (Tokyo, Japan) 1200 series HPLC
27 pump fitted with an HDC 5-300 Type-1 column (linearity range from 5 to 300 nm) from the same
28 supplier. Sample injections were performed manually using a 100 μL loop and an inert Rheodyne
29 injection valve. The elution was performed in isocratic mode at a flow rate of 1.0 mL min^{-1} . An ICP-
30 MS detector model 7500cx from Agilent Technologies was coupled on-line to the chromatographic
31 system by using a polypro nebulizer mounted on a double-pass Scott spray chamber thermostated
32 at 2°C. The instrument operated at 1500 W RF power with a carrier gas flow rate of 1.1 mL min^{-1}
33 and make up gas flow rate of 0.1 mL min^{-1} . The lens voltages were tuned daily for best sensitivity
34 using a 1 ng mL^{-1} solution of Ag. In order to minimize the matrix effects, robust plasma conditions
35 were achieved by keeping oxides and double charges rates below 2 % based on the response of a
36 Ce 1 ng mL^{-1} solution, and using 8 mm of sample depth. Acquisition was carried out by monitoring
37 both the isotopes of Ag (m/z 107 and 109) with a dwell time of 5 ms. Automatic correction for the
38 dead time was adopted, the parameter was estimated as reported elsewhere [33]. A settling time
39 of 2 ms was automatically selected by the instrument and was taken into account to correct the
40 calibration of NPs number concentration, as reported below.

41
42 Synchrotron radiation μXRF and Ag L_{III} -edge μXANES measurements were performed using the
43 scanning transmission X-ray microscope of beamline ID21 at the European Synchrotron Radiation
44 Facility (ESRF, Grenoble, France). Details on standards/sample preparation, instrumental
45 parameters and data elaboration for μXRF and μXANES are provided as supporting information.

46 Data elaboration

47
48 Data treatment for HDC-splCP-MS was carried out by using a home-made program written in
49 Fortran language and run using the compiler Compaq Visual Fortran (Compaq Computer
50 Corporation). The program reads the ICP-MS raw data file directly and provides a number of
51 output files including overall statistics and matrices. The latter were directly imported in Surfer 11
52 (Golden Software) for graphical elaboration of the contour plots (3D chromatograms). Excel
53
54
55
56
57
58
59
60

1
2
3 spreadsheets (Microsoft), OriginPro 8.5 (OriginLab) and Statistica 10 (StatSoft) were used for
4 additional calculations and graphical elaboration. PyMca [34] and Athena [35] software were used
5 to elaborate the μ XRF and μ XANES data.
6

7 **2. Results and discussion**

8 **2.1. Implementation of data analysis**

9 *2.1.1. Dwell time and data pre-processing*

10
11
12 The limit of detection (LOD) in spICP-MS has two possible interpretations: as the lowest detectable
13 particle size (LOD_S^{NP}) and the lowest detectable particle number (LOD_N^{NP}). Measuring
14 simultaneously the dissolved Ag introduces also a third definition, which is the lowest detectable
15 concentration of this fraction (LOD_C^{D}). The choice of the dwell time is the key to determine all
16 these parameters in samples where both NPs and dissolved Ag are present, and the overall
17 statistical reliability of the results in spICP-MS. Individual NPs in ICP-MS generate transient signals
18 with a temporal width of 0.3-0.5 ms [36]. Recent instrumentation allows setting the dwell time
19 within the μ s range, so that single events can be described by multiple data points. This results in a
20 significant reduction of the background, a decreased LOD_S^{NP} and an improved range of number
21 concentration [37]. However, the same increase in the signal-to-background ratio is expected to
22 make more difficult the determination of the dissolved Ag by statistical deconvolution within the
23 same analysis, increasing the LOD_C^{D} . Moreover, with μ s dwell times, the probability to observe split
24 of events between adjacent time windows must be taken into account [30], and the electronic and
25 computational load due to data size can be potentially problematic when applied to hyphenated
26 techniques, where the acquisition lasts for tens of minutes. Conversely, conventional ms dwell
27 time leads to higher LOD_S^{NP} and requires higher dilution of the samples to avoid detecting multiple
28 events within the same time window [30], but it is more suited for performing the simultaneous
29 determination of dissolved Ag and using hyphenated instrumental approaches. According to other
30 authors, a dwell time in the range of 3-5 ms is adequate to achieve good quality data in our
31 context [38]. The minimum dwell time that can be set on our instrument for the acquisition of a
32 single m/z is 10 ms, but a dwell time of 5 ms can be chosen by monitoring both masses of Ag. This
33 required a data pre-processing step for normalization of the two signals to the relative natural
34 abundance of each respective isotope, before merging them into a single chromatogram. Given
35 the proximity of the two abundances (0.518 for ^{107}Ag and 0.482 for ^{109}Ag), the difference in signal
36 intensity for the two masses is negligible at low counting rates, but was nevertheless taken into
37 account when applying the threshold in the following deconvolution step. In addition, the
38 acquisition of two masses introduces a settling time, which slightly affects the number of detected
39 particles (see section 2.1.4.).
40
41
42
43
44
45
46
47

48 *2.1.2. Deconvolution of the signals*

49 The expected forms of dissolved Ag in plasma (protein complexes) have hydrodynamic diameters
50 smaller than the LOD_S^{NP} (see section 2.1.4.), and close to the lower limit of separation range. Given
51 also the poor resolving power of HDC, their peak cannot be chromatographically resolved from
52 those of ~ 20 nm particles, thus making deconvolution a necessary operation. In this work, the
53 statistical deconvolution of the signals from dissolved Ag species and AgNPs was based on a
54 nonparametric statistical test applied to each data point of the chromatogram as it was
55 sequentially scanned. The intensity value of each point was compared to that of its two adjacent
56 neighbours, and their difference was calculated. If at least one of the two differences overcame a
57 threshold value given by the maximum expected difference between any data generated by
58
59
60

dissolved Ag, the hypothesis of the point being associated to dissolved forms was rejected. For each pair of points to be compared, the relative threshold value was specifically calculated as a negative exponential function of the lower of the two intensities. The function was externally calibrated on the chromatogram of a single standard of dissolved Ag with a relatively high concentration (500 pg mL⁻¹) using the following procedure. The chromatogram was divided into consecutive windows of 2 s width, in which the signal was assumed to be stationary. For each window, the empirical distribution of the data was calculated to extract the 1st-to-99th interpercentile range. The range was plotted against the average value within the same window as shown in Fig. 1a. The interpercentile range can be interpreted as the maximum difference in signal intensity between two data points generated by dissolved Ag at a 98 % confidence level, and was adopted here as the threshold value to discriminate the signals. The vector of points for which the hypothesis of being generated by dissolved Ag was rejected, constituted the NPs extracted chromatogram.

2.1.3. Elaboration of the 3D NPs raw chromatogram

The NPs chromatogram was firstly treated by converting the normalized signal intensities into their cube square. This step was necessary to obtain final chromatograms in which the mass-derived diameter is represented on a scale with uniform resolution. In a second step, the dimensions of elution time and normalized signal intensity were gridded into windows of selected width according to the procedure proposed by Pergantis et al. [28]. The width of the intensity windows was fixed at 0.6266 normalized counts^{1/3}, resulting in a resolution of 6.5 nm for the mass-derived diameter after calibration. The width of the elution time windows was fixed at 5 s in order to contain 714 data points to guarantee statistical representativity. After gridding, the number of events detected within each window was counted, and a raw 3D chromatogram was yielded as a 3-columns matrix consisting of the central values of the elution time (x-axis) and the normalized events' intensity (y-axis), and the number of detected events (z-axis) for each window.

2.1.4. Calibrations and elaboration of the 3D NPs final chromatograms

Besides the threshold function, other external calibrations based on the injection of monodisperse NPs standards were necessary to convert the normalized signal intensity into mass-derived diameter, and the elution time into hydrodynamic diameter. Standard suspensions with a 20, 40, 60 and 100 nm nominal size and variable concentration were injected to calibrate these two parameters as done by Pergantis et. al. [28]. For each standard, the mode of the 3D raw chromatogram provided the data to be included in the calibration curves, which are shown in Fig. 1b,c. A LOD_S^{NP} of 16 nm was calculated as 3 times the standard error of the intercept of the mass calibration curve. This value is in agreement with the range of those estimated by other authors both theoretically and experimentally (in water samples) using spICP-MS [22]. The extrapolation of the number concentration of AgNPs in a sample required estimating separately their transport efficiency through the nebulization system. Adapting the formula by Pace et al. [39], the overall number of detected particles n_r of radius r , using the hypothesis of purely metallic and spherical particles, can be expressed as:

$$n_r = \eta \cdot \frac{c_r^m}{\frac{4}{3}\pi r^3 \rho} \cdot v \cdot \frac{t_i}{t_s + t_i} \quad \text{eq.1}$$

where η is the transport efficiency (independent by the radius), c_r^m is the mass concentration of the NPs (pg mL⁻¹), v is the injection volume (mL), ρ is the density of Ag in pg nm⁻³ = 1.049 · 10⁻⁸, t_i is the integration time and t_s is the settling time. The transport efficiency can be estimated by analyzing a series of standards of any radius at different known mass concentrations, calculated as the slope of the regression line in eq. 1. However, one should note that even if approximately

monodisperse, a standard suspension still has a characteristic size distribution which may be not perfectly symmetric, particularly for the size ranges close to the LOD_S^{NP} , so that simple counting the overall number of detected particles would introduce a bias. In order to overcome this potential problem, we used the calibration of mass-derived diameter to convert the number of detected particles into a mass for each window of the raw chromatogram. Summing the mass of all windows provided the total detected mass of Ag, to be used in place of n_r for efficiency estimation. The method was tested on four nominal particles sizes, as shown in Fig. 1d. Consistently with the independence of η from the particles' size, an average value of $1.78 \pm 0.07\%$ was obtained for the four calibrations. If a minimum number of 3 detected particles is arbitrarily adopted as the statistical threshold to verify their presence, taking into account the transport efficiency, settling time and injection volume, a LOD_N^{NP} of ~ 2300 particles mL^{-1} is achieved. This threshold can be indifferently adopted for all particles or for specific size classes. Finally, a calibration was also required for the dissolved Ag fraction by injecting standards of ionic Ag with variable concentration as shown in Fig. 1e, obtaining a LOD_C^{D} of 13 pg mL^{-1} .

All calibrations reported above allowed to convert the data of the 3D NPs raw chromatogram for each sample into a final chromatogram representing the experimental distribution of NPs in terms of number concentration or mass concentration depending on the hydrodynamic diameter and mass-derived diameter.

2.2. Stability of the AgNPs in the mother standards and in mobile phase.

The mother citrate-stabilized dispersions were stored at 4°C and no significant changes in their size distribution were noticed after more than 1 year (as observed by TEM). In addition, no peaks of dissolved Ag were detected by HDC-ICP-MS when injecting single standards freshly diluted in mobile phase for calibration within the same time span. The temporal stability of AgNPs standards in the mobile phase below the ng mL^{-1} level was also checked. Despite the appearance of small peaks of dissolved Ag was observed after leaving the vials exposed to light and room temperature up to 24 h, the corresponding concentration was below the LOD_C^{D} for all particle sizes. Nevertheless, in order to avoid any potential alteration of the dynamics of AgNPs due to interaction with the mobile phase, all standards for calibration were always prepared freshly from the mother dispersion and immediately injected, all samples were analysed immediately after preparation, and replicates were obtained from independent preparations rather than from repeated injections.

2.3. Dynamics of AgNPs incubated in human plasma

The developed method was used to study the dynamics of AgNPs in human plasma. Standards with nominal diameters of 20, 40, 60 and 100 nm were mixed in whole plasma at concentrations of 10, 16, 37 and 100 ng mL^{-1} , respectively, sonicated for 1 min and then incubated for 2 h. After incubation, the sample was diluted 20-fold in the mobile phase and directly injected without further sonication. A control sample was prepared by diluting the AgNPs mixture in the mobile phase at the same final concentration, followed by sonication for 1 min, and direct injection. Fig. 2 shows the final 3D chromatograms obtained for the control and plasma incubated mixtures. A number of significant changes were observed in the distributions of NPs after 2 h of incubation in plasma: i) a slight general decrease in the mass-derived diameter; ii) a significant decrease in the number and mass concentration of the NPs; iii) a generalized shift in the distribution towards the higher hydrodynamic diameters of 10-20 nm. While the first two effects can be ascribed to a partial dissolution of the NPs, the increased hydrodynamic diameter is compatible with two possible phenomena: agglomeration of NPs and the formation of a protein corona onto their surface. The agglomeration of uncapped NPs is a feasible process in plasma, particularly due to the

1
2
3 relatively high ionic strength of the medium [3]. We did not observe the appearance of new
4 modes in the mass-derived diameter corresponding to multiples of the nominal diameters of 40,
5 60 and 100 nm. However, agglomeration effects cannot be excluded for the 20 nm particles due to
6 the theoretical superimposition of the multiples of their mass on the modes of the other
7 standards. Conversely, the formation of a proteins corona is a plausible generalized process,
8 particularly due to the interaction of thiol groups in amino acids with the charged surface of AgNPs
9 in a medium with a high ionic strength [40,41].

10
11 In order depict the temporal dependence of the dynamics of AgNPs in human plasma, the
12 standard suspension with a 100 nm size was selected for further incubation experiments. An
13 aliquot of the mother monodisperse suspension ($20 \mu\text{g mL}^{-1}$) was sonicated for 1 min, then mixed
14 1:1 with plasma and incubated for 24 h. At time steps of 2, 4, 6, 8, 16 and 24 h, aliquots of the
15 solution were collected, diluted 10,000-fold in the mobile phase, and analyzed immediately. Fig.
16 3a shows that the dissolution of AgNPs is not linearly time-dependent on an hourly scale in a
17 closed system. The most significant change was observed between the 4 and 8 h incubations, with
18 a decrease in the molar fraction of Ag present in the original form of NPs, corresponding to the
19 appearance and increase of the dissolved fraction. Between 16 and 24 h the molar fractions seem
20 to reach equilibrium. The precision of detection efficiency ($\sim 4\%$ of relative error, see paragraph
21 2.1.), which affects the estimated number concentration, is the dominant source of uncertainty for
22 AgNPs molar fraction. The calibration of dissolved Ag is more reproducible because the relative
23 error of the slope of its calibration curve (Fig. 1e) is 1%. The mass-derived diameter of the
24 particles exhibits a substantial linear decrease from 100 to 80 nm in 24 h (Fig. 3b), confirming the
25 partial dissolution of the individual particles. In this case, the standard deviation among replicates
26 is zero because their differences are smaller than the width of the signal intensity windows
27 adopted for gridding (see paragraph 2.1.3.). Thus, for each estimated diameter d , the width of the
28 gridding windows $\pm 6.5/d\%$ can be considered as the maximum theoretical uncertainty, and was
29 taken to represent the whiskers in Fig. 3b.

30
31 Speciation analyses by μXANES were carried out on analogously incubated samples. Standards of
32 AgNPs with a 10 nm size ($20 \mu\text{g mL}^{-1}$) and ionic Ag solution (nitrate, $10 \mu\text{g mL}^{-1}$ as Ag) were
33 incubated in a water solution containing HSA ($\sim 0.5 \text{ mg mL}^{-1}$) and in whole plasma. After 2 h a drop
34 of each solution was freeze-dried between Ultralene[®] windows and was directly analyzed by
35 μXANES . Representative spectra for each of the incubated standards and pure species of Ag, as
36 shown in Fig. 4a-b, allowed us to identify the chemical forms of Ag after incubation and their
37 relative molar fractions estimated by linear combination fitting (LCF), as reported in Table 1. The
38 μXANES analysis showed that after 2 h of incubation in HSA the Ag^+ ions were mostly complexed
39 by thiols (represented by the Ag-GSH bound). Conversely, AgNPs remained intact almost
40 quantitatively, even if Ag-thiols were also detectable. This confirms that the formation of a protein
41 corona on the surface of AgNPs has a major inhibiting effect on their dissolution in the short term.
42 Differently, in whole plasma, the early dynamics of Ag were dominated by chlorides, with
43 formation of insoluble AgCl from free Ag^+ , and significant agglomeration of the AgNPs, as marked
44 by the high weight of the metallic Ag foil spectrum obtained by LCF.

51 **2.4. Dynamics of AgNPs agglomerates released from a dressing incubated in human plasma**

52
53 The 2 h incubation experiment in whole plasma was carried out also by using the intact dressing
54 Acticoat Flex3[™]. The dressing consists of a net of polyethylene fibers, individually and uniformly
55 coated with a layer of uncapped AgNPs of 10 nm size; other characteristics of the product can be
56 found elsewhere [33]. Previous experiments showed that the dressing releases AgNPs as
57 agglomerates with widely variable size *in vitro* in human serum substitute [42], and agglomerates

1
2
3 were also detected in the fibroblasts of burnt patients after 7 days of treatment [32]. In this
4 experiment, 2.45 mg of the dressing (0.32 mg as Ag) were dipped into 1 mL of whole plasma and
5 sonicated for 10 min to accelerate the release of AgNPs as individual particles or small
6 agglomerates. After 2 h of incubation, the plasma was centrifuged at 3000 rpm for 10 min in order
7 to remove the fibers, cloth debris and micrometric agglomerates of AgNPs, then an aliquot was
8 diluted 100-fold in the mobile phase and directly injected into the chromatographic system. The
9 3D chromatograms in Fig. 5a-b show a few particles with size >16 nm, corresponding to small
10 agglomerates of 2-5 NPs with 10 nm size. Significantly higher hydrodynamic diameters, with
11 respect to the mass-derived diameter, were also observed. The latter effect supports the
12 hypothesis that the observed particles are small (non-spherical) agglomerates, and is also
13 compatible with additional proteins capping effects. The dissolved Ag fraction resulted lower than
14 the LOD_C^D.

15
16
17 A 20 μ L aliquot of the same sample after incubation was collected before centrifugation, was
18 freeze-dried and analyzed by μ XRF and μ XANES. Preliminary μ XRF mapping of the sample allowed
19 us to detect a number of micrometric agglomerates of AgNPs or fragments of the dressing. A
20 region surrounding one of the particles was selected, and the distribution of Ag, Cl and S was
21 mapped as shown in Fig. 6a. A characteristic non-uniform accumulation of Cl was observed at the
22 border of the Ag particle, while S was uniformly distributed in the surrounding medium. μ XANES
23 spectra were collected in the same region for each pixel to be individually elaborated by LCF in
24 order to extract a coarse estimation of the molar fraction of the three main expected species:
25 intact AgNPs, AgCl and Ag-thiols. The resulting μ XANES map is shown in Fig. 6b. Although total Ag
26 and Cl presented widely different distributions, a relatively uniform distribution of the Ag species
27 was observed, consistent with the participation of the whole surface of the AgNPs agglomerates in
28 the chemical dynamics of the metal. The average molar distribution of the species within the
29 entire region was 49 % AgCl, 22 % AgNPs and 20 % Ag-thiols (9 % unidentified species). The overall
30 distribution was also estimated by firstly merging all the spectra within the region, and then
31 performing the LCF on the pooled spectrum. This procedure allowed us to weight the contribution
32 of each pixel on the base of the total Ag level, and provided the values: 53 % AgCl, 31 % AgNPs and
33 15 % Ag-thiols. Compatibly with Fig. 6b, the slight variations with respect to the previous
34 estimation are consistent with a major localization of AgCl and AgNPs in the regions with elevated
35 Ag level, while Ag-thiols are mainly present in the peripheral areas. The assignment of previously
36 unidentified species could also have affected the latter values. The co-presence and relative
37 proportion of the three species reveal that the dynamics of AgNPs in plasma involve integrated
38 and complex processes. Free Ag ions are expected to be a negligible fraction in biological systems
39 due to the high formation constant for chloride and thiol bonds [43,3], so that dissolution and
40 formation of complexes may take place directly on the surface of the AgNPs as an integrated
41 process. Properties of the medium such as its general composition, concentration of chloride and
42 pH, and kinetics of complexation influence the dynamics. Although protein thiols should be
43 thermodynamically favoured for Ag binding in plasma with respect to chlorides [6,3], our data
44 support the hypothesis that the latter have a kinetic advantage when interacting with Ag ions
45 directly on the charged surface of the bare NPs, leading to an early effect of partial dissolution,
46 and possibly agglomeration of the smallest NPs. Still, protein thiols may co-participate to these
47 dynamics by enclosing the particles and superficial chlorides, inhibiting further interactions with
48 the medium, the removal of AgCl from the surface and further agglomeration effects. Given the
49 affinity of thiols for Ag, subsequent displacement of the metal from the chlorides is likely, resulting
50 in its final mobilization. In agreement with Liu et al. [3], thiols binding appears to be the limiting
51 process in regulating the dissolution of AgNPs in plasma, and the mediator for systemic
52
53
54
55
56
57
58
59
60

distribution of the metal, but our findings suggest that kinetic factors play a crucial role in this complex dynamics.

2.5. Whole blood from burnt patients treated with a AgNPs-containing dressing

In addition to the temporal dynamics of the chemical transformations of AgNPs, the particles could also undergo simultaneous mobilization through the tissues, with consequent change in the properties of the surrounding medium. The formation of a proteins corona is probably the main favouring factor for the cellular uptake on AgNPs [41], which has been observed in human skin both *in vitro* and *in vivo* in burnt patients [32]. However, the few available experimental data suggest that the metal has a poor capability to penetrate the skin in depth, even if penetration may be enhanced in damaged tissue [32,44].

In order to evaluate the actual potential of AgNPs to reach the bloodstream before dissolution, we used HDC-spICP-MS to analyze four whole blood samples collected from three adult patients (A-C) treated for mid-thickness skin burns with a single application of the dressing. The main clinical information is summarized in Table 2. The patients had a comparable % of burned body surface, which represents the wound area exposed to AgNPs. Three blood samples were collected from distinct patients 3 days after the application; and an additional sample was collected from patient A after 6 days of treatment. Compatibly with our previous estimations that the dose of Ag released by the dressing into the patient's tissues *in vivo* would be elevated [33], a significant level of total circulating Ag was observed in all patients after 3 days of application of the dressing (Table 2). The values ranged between ~ 30 to 80 ng mL^{-1} and were more than 2 orders of magnitude higher than the baseline level in an unexposed population [45], and slightly lower than those observed in the serum of paediatric burnt patients treated with the same dressing (average 114 ng mL^{-1}) [46]. Differently from the latter cited work, we did not observe any apparent correlation between blood Ag and the percentage of burnt body area, and just a slight increase in Ag was noticed after 3 additional days of application for patient A.

An aliquot of the blood was then centrifuged at 3000 rpm for 10 min to remove the cell debris in order to avoid clogging the chromatographic system. The supernatant was recovered and analyzed for total Ag. The average recovery of total Ag after centrifugation was $\geq 96 \%$ for all samples except patient C (76 %), and a minimal loss of Ag due to co-precipitation was therefore assumed for most cases. The possibly co-precipitated Ag can be ascribed to its association to cellular debris and large biomolecules whose size exceeds the effective separation range of the HDC system. Based on the total concentration of Ag, the centrifuged samples were diluted in the mobile phase according to specific dilution factors (see Table 2), optimized to obtain the same final concentration of $\sim 400 \text{ pg mL}^{-1}$ of Ag. This target value was selected from preliminary tests as the optimum concentration for detecting a significant number of AgNPs with a mass-derived size close to the LOD_S^{NP} under the hypothesis that they were present as a significant molar fraction of Ag ($> 10 \%$).

We did not detect any significant event associated to AgNPs agglomerates $>16 \text{ nm}$ in the four blood samples (chromatograms are not shown). Conversely, from the chromatograms of dissolved Ag shown in Fig. 7, an average molar fraction of $94 \pm 9 \%$ was estimated for the dissolved species (see Table 2), which is not statistically different from the total level of the metal.

Considering that: i) our previous studies have shown that in burnt patients treated with Acticoat Flex3TM, AgNPs are released as agglomerates and maintain this form even in the tissue; ii) a poor dermal penetration of PVP-coated AgNPs, restricted to small ($<30 \text{ nm}$) particles in damaged skin, was observed *in vitro* [44]; and iii) we documented here that small AgNPs exhibit both agglomeration and partial dissolution effects at an hourly time scale in plasma; the results of blood

analysis strongly support the hypothesis that the systemic mobilization of Ag is driven by the *in situ* dissolution of NPs in the skin. The first medium entering in contact with the AgNPs released by the dressing onto the wound bed is the exudate, whose composition is similar to the serum. This medium is the major candidate to host the *in situ* transformations of AgNPs, where dissolution may be also enhanced by the lower pH (5.7), typical of the inflammatory phase in wounds [47]. It is also likely that the reduced blood circulation in burns further inhibits the dispersion of AgNPs. However, let us keep in mind that the specific local characteristics of the wound may dramatically affect the release of AgNPs from the dressing and the composition/production/turnover of the exudate. This can lead to significantly different AgNPs dynamics at a local level, resulting in the possible penetration of agglomerates into the shallow tissue layers. Photochemical reduction of Ag complexes with formation of secondary Ag/S/Se particles can also occur in the skin [3]. We previously observed a few electron-dense particles in skin biopsies after application of the dressing, which are potentially representative of photoprecipitation [32]. However, this phenomenon appears to be limited to the most severe lesions, which require long-term treatments and replacement of the dressing, leading to exposure to light and an increased Ag dose.

3. Conclusion

The exponentially growing market of consumer and medical products containing AgNPs has raised the urgent need for regulatory standards targeted at health and safety. Developing adequate analytical methods to achieve detection and characterization of AgNPs and their ionic counterpart in biological media is the key requisite to support regulatory requirements with robust scientific evidence.

An innovative method is proposed here for the simultaneous determination of dissolved Ag and the characterization of AgNPs in human plasma and blood. By coupling HDC separation, spICP-MS detection and a dedicated algorithm for data elaboration, comprehensive information on the chemical state of the Ag⁺/AgNPs system can be retrieved in a single analytical run. While HDC separates the NPs based on their hydrodynamic diameter and spICP-MS provides information on their mass distribution, both techniques have the potential to discriminate physically and statistically (respectively) the signal of NPs from that of dissolved Ag, but this advantage was not exploited before. We combined the two techniques and a home-made software based on a new algorithm able to process the raw ICP-MS chromatogram for deconvoluting the signal of dissolved Ag from that of AgNPs. From a single injection, the method provides the chromatogram and concentration of dissolved Ag; the distribution of NPs in terms of hydrodynamic diameter, mass-derived diameter, size-dependent number of detected NPs; the total number concentration and size-dependent mass concentration of the NPs. A variety of 3D chromatograms can be obtained from the results to achieve a comprehensive characterization of AgNPs.

The method is robust when applied to heavy matrices such as plasma and blood, and in principle can be extended to other biological media and to other metallic NPs. The algorithm in particular is suitable for the deconvolution and determination of particulate and dissolved fractions independently by the element, or just for the removal of non-stationary background in any separation technique coupled to spICP-MS.

Combining the method with μ XANES speciation and imaging provides an integrated approach which opens the way to elucidate the dynamics of AgNPs in biological fluids or extracts *in vivo* under realistic conditions (real human subjects, real administered doses).

We applied this strategy to study the behaviour of AgNPs standards and of an AgNPs-coated dressing incubated in human plasma, and to investigate for the first time the capability of AgNPs to reach the systemic circulation after topical application to burnt patients.

The results showed that partial dissolution of uncoated AgNPs takes place in plasma on an hourly time scale with nonlinear dynamics in a closed system. Chlorides and protein thiols co-participate in the process through complex temporal and spatial mechanisms, forced by kinetic factors. The early dynamics and dissolution of AgNPs are dominated by interaction with chlorides directly on their surface. Formation of a protein corona takes place in the meantime, resulting in the inhibition of further reactions with the medium, slower displacement of Ag from chlorides and final mobilization of the metal. As a whole, thiols binding is proposed as the main regulator of AgNPs dissolution in plasma and of the systemic distribution of the metal. The analysis of whole blood from burnt patients suggested that the dynamics of AgNPs dissolution after topical administration takes place mainly *in situ*, most probably in the exudate, so that their potential to undergo systemic distribution in the intact form is minimal. Further studies are currently in progress to investigate the chemical speciation of Ag directly in wound tissues.

Acknowledgments

The authors are grateful to the Italian Ministry of Education, University and Research for financial support through the project MIUR-FIRB number RBF08M6W8. The European Synchrotron Radiation Facility is acknowledged for provision of beamtime at ID21. ELGA LabWater is acknowledged for providing the PURELAB Option-Q and Ultra Analytic systems, which produced the ultra-pure water used in these experiments. Francesca Benetello and Bruno Pavoni from Ca' Foscari University of Venice are acknowledged for the lyophilisation of standards and samples.

Disclaimer: The authors declare that they have no conflict of interest.

Appendix

Characterization of the commercial AgNPs standards dispersions

The morphological characterization of the mother AgNPs standard dispersions was carried out by TEM using a Tecnai 12 G² instrument (FEI, USA). For the analysis, a 3 μL drop of each dispersion was deposited on a support Formvar/Carbon on 200 mesh thick grid, let dry at room temperature and directly analysed. The images were acquired at 120 kV high voltage and using tungsten filament, twin optics and an Olympus side-mounted camera. The software ImageJ (National Institutes of Health, USA) was used for particles' counting and shape characterization. Representative TEM images of the standard NPs and a summary of their size/shape parameters are shown in Fig. 8 and reported in Table 3, respectively.

The z-potential was measured by using a Zetasizer Nano (Malvern, UK) at 24°C in DTS1070 cells pre-washed with a citrate 60 $\mu\text{g mL}^{-1}$ water solution. For the analysis, each standard suspension was sonicated for 5 min, equilibrated for 120 s in the cell, and 5 replicate measurements of 10 to 100 readings were acquired. The z-potential of the standard NPs is also reported in Table 3.

Total mass concentration of Ag in the standards was measured by ICP-MS *previa* dissolution in HNO_3 5% v/v and subsequent dilution in NH_4OH 2.8 % w/w. The analysis was carried out in full-quant mode by external calibration with Rh as internal standard.

Methods for μXRF and μXANES analyses

Standards and samples

Solid-state reference compounds for μ XANES included: Ag⁰ foil, AgCl, Ag₂SO₄, AgNO₃, Ag₂O, Ag sulfadiazine (AgSD) and a fragment of intact dressing Acticoat Flex3TM. Reference standards of Ag⁰NPs 10 and 100 nm were prepared from mother water suspensions (citrate stabilized, 20 μ g mL⁻¹ as Ag) by deposition of a 20 μ L drop between Ultralene[®] windows and microscopy slides, followed by rapid freezing and freeze-drying for 24 h. A standard of Ag bonded to GSH was prepared by incubating ionic Ag (from AgNO₃, 10 μ g mL⁻¹ as Ag) in a water solution of GSH \sim 0.5 mg mL⁻¹, at 37° C under gentle shaking for 2 h and in dark conditions, followed by freeze-drying as reported above. Standards of Ag⁰NPs 10 nm, ionic Ag and the intact dressing Acticoat Flex3TM (2.45 mg fragment) were also incubated in a water solution containing HSA, (\sim 0.5 mg mL⁻¹) and in whole human plasma, freeze-dried as reported above, and analyzed as unknown samples.

Instrumental parameters and data elaboration

The μ XRF and Ag L_{III}-edge μ XANES measurements were performed using the scanning X-ray microscope of beamline ID21 at the European Synchrotron Radiation Facility (ESRF, Grenoble, France), working at room temperature conditions. Detectors included a Si₃N₇ diode for I₀ and an 80 mm active area Silicon Drift Detector (Bruker) for the emitted fluorescence. Focusing was achieved using fixed curvature Kirkpatrick-Baez mirror optics. The photon flux was 3.6 x 10⁹ ph s⁻¹ at 3.42 keV with a beam size of 1.0 x 1.2 μ m².

μ XRF maps of signal intensities for individual elements (Ag, S and Cl) were collected for preliminary analysis to select optimal regions for the subsequent μ XANES analysis. The μ XRF maps were acquired with variable lateral resolution (0.5 to 2 μ m) and integration time of 100 ms. The raw data (counts) were elaborated using the PyMca software as follows: i) correction for the settling time and conversion to counts per second (cps); ii) deconvolution (batch fitting of the μ XRF spectra); iii) normalization for the incident beam flux.

Batch Ag L_{III}-edge μ XANES spectra of 30 s were collected and averaged for each spot of interest from 3.32 to 3.42 keV energy range with 0.5 eV steps. The beam position was slightly moved from one spectrum to another to avoid radiation damage. At least 10 spectra were averaged for each region of interest. After background removal and normalization, the spectra were calibrated by taking the first inflection point of at 3.3545 keV and then smoothed by interpolation with 5 iterations. The μ XANES spectra of Acticoat Flex3TM and HSA/plasma incubated standards were treated by LCF using the Athena Software with the following set of reference spectra as independent variables: Ag⁰ foil, Ag⁰NPs 10 nm, AgCl, Ag₂SO₄, AgNO₂, Ag₂O, AgSD and AgGSH. A linear term was allowed to compensate for small differences in data normalization, no energy shift was allowed, and weights and their sum were forced to sum to 1. The energy range used for fitting was 3.3345 to 3.4145 keV (e0 - 0.02 to e0 + 0.06). The quality of fitting was quantified by the normalized sum-square residuals $NSS = \frac{\sum(\mu_{\text{experimental}} - \mu_{\text{fit}})^2}{\sum(\mu_{\text{experimental}})^2} \times 100$, where μ is the normalized absorbance. Linear combinations of one, two and three reference standards were examined. The best fit with n+1 components was retained if NSS was decreased by more than 15 % as compared to the best fit using n components. Based on the results, four main Ag species were revealed in the samples: Ag⁰ foil, Ag⁰NPs 10 nm, AgCl and AgGSH; the other minority species were pooled as "other". When two or more fits of equivalent quality (relative difference of NSS < 10 %) were obtained with different combinations of such a minority species, proportions and NSS were expressed as mean percentage with standard deviation (SD) between brackets, calculated for the equivalent fits.

The μ XANES spectra acquired in fluorescence mapping mode by scanning the beam with a 2 x 2 μ m² step size and a 50 ms dwell time per pixel with 3 eV energy steps in the region from 3.320 KeV

1
2
3 to 3.341 KeV, 0.5 eV from 3.341 KeV to 3.381 KeV, and 1 eV from 3.382 KeV to 3.42 KeV. This
4 resulted in a total of 126 images recorded using a region of interest selective for Ag L3M4 and
5 L3M5 emission lines, corrected for detector dead time (always kept below 20%) and normalized by
6 the incident beam flux. The stack of images was converted to an hdf5 file containing intensities
7 and the energy values for each map to be processed using PyMca for μ XANES spectra extraction.
8 The map was treated by moving merge of the spectra on 2 x 2 pixels areas and with 1 pixel step, in
9 order to reduce the noise and improve the statistical representativity. After background removal
10 and normalization, the spectra were calibrated and individually processed by LCF as above, but
11 using only the reference spectra of Ag⁰NPs 10 nm, AgCl, and AgGSH as independent variables.
12 Based on visual inspection of the fits, an arbitrary threshold of NSS < 0.1 was adopted to remove
13 from the map the pixels with insufficient quality of the fit. A number of pixels in the upper right
14 side of the map (see Fig. 4b) were discarded based on this criterion. These pixels were affected by
15 the sharp change in intensity at the border of the analyzed particle coupled to beam drift caused
16 by scanning the energy with the double crystal monochromator. The retained pixels were re-
17 processed by LCF testing all combinations in which one of the three reference standard was
18 removed. Each standard was considered significant if its introduction decreased the NSS by more
19 than 3 %. This threshold was calibrated *a posteriori* to guarantee that all pixels in the map had at
20 least one significant component, and a coefficient equal to zero was assigned to the non
21 significant components. For each pixel, the coefficients were finally multiplied for the
22 corresponding signal intensity of total Ag (from the μ XRF map), also treated by the moving merge
23 procedure, to obtain the absolute contribute of each species expressed in cps.
24
25
26
27
28
29
30
31
32
33
34
35
36
37
38
39
40
41
42
43
44
45
46
47
48
49
50
51
52
53
54
55
56
57
58
59
60

References

1. Rigo C, Ferroni L, Tocco I, Roman M, Munivrana I, Gardin C, Cairns WRL, Vindigni V, Azzena B, Barbante C, Zavan B (2013) Active Silver Nanoparticles for Wound Healing. *Int J Mol Sci* 14 (3):4817-4840.
2. Wilkinson LJ, White RJ, Chipman JK (2011) Silver and nanoparticles of silver in wound dressings: a review of efficacy and safety. *J Wound Care* 20 (11):543-549.
3. Liu J, Wang Z, Liu FD, Kane AB, Hurt RH (2012) Chemical Transformations of Nanosilver in Biological Environments. *ACS Nano* 6 (11):9887-9899.
4. Reidy B, Haase A, Luch A, Dawson KA, Lynch I (2013) Mechanisms of Silver Nanoparticle Release, Transformation and Toxicity: A Critical Review of Current Knowledge and Recommendations for Future Studies and Applications. *Materials* 6 (6):2295-2350.
5. Gnanadhas DP, Ben Thomas M, Thomas R, Raichur AM, Chakravorty D (2013) Interaction of Silver Nanoparticles with Serum Proteins Affects Their Antimicrobial Activity In Vivo. *Antimicrob Agents Chemother* 57 (10):4945-4955.
6. Liu J, Sonshine DA, Shervani S, Hurt RH (2010) Controlled Release of Biologically Active Silver from Nanosilver Surfaces. *ACS Nano* 4 (11):6903-6913.
7. You CG, Han CM, Wang XG, Zheng YR, Li QY, Hu XL, Sun HF (2012) The progress of silver nanoparticles in the antibacterial mechanism, clinical application and cytotoxicity. *Mol Biol Rep* 39 (9):9193-9201.
8. Pyrz WD, Buttrey DJ (2008) Particle Size Determination Using TEM: A Discussion of Image Acquisition and Analysis for the Novice Microscopist. *Langmuir* 24 (20):11350-11360.
9. Luo P, Morrison I, Dudkiewicz A, Tiede K, Boyes E, O'Toole P, Park S, Boxall AB (2013) Visualization and characterization of engineered nanoparticles in complex environmental and food matrices using atmospheric scanning electron microscopy. *J Microsc* 250 (1):32-41.
10. Grobelny J, DelRio F, Pradeep N, Kim D-I, Hackley V, Cook R (2011) Size Measurement of Nanoparticles Using Atomic Force Microscopy. In: McNeil SE (ed) *Characterization of Nanoparticles Intended for Drug Delivery*, vol 697. *Methods in Molecular Biology*. Humana Press, pp 71-82. doi:10.1007/978-1-60327-198-1_7
11. Hagendorfer H, Kaegi R, Parlinska M, Sinnet B, Ludwig C, Ulrich A (2012) Characterization of Silver Nanoparticle Products Using Asymmetric Flow Field Flow Fractionation with a Multidetector Approach – a Comparison to Transmission Electron Microscopy and Batch Dynamic Light Scattering. *Anal Chem* 84 (6):2678-2685.
12. Proulx K, Wilkinson KJ (2014) Separation, detection and characterisation of engineered nanoparticles in natural waters using hydrodynamic chromatography and multi-method detection (light scattering, analytical ultracentrifugation and single particle ICP-MS). *Environ Chem* 11 (4):392-401.
13. Mitrano DM, Barber A, Bednar A, Westerhoff P, Higgins CP, Ranville JF (2012) Silver nanoparticle characterization using single particle ICP-MS (SP-ICP-MS) and asymmetrical flow field flow fractionation ICP-MS (AF4-ICP-MS). *J Anal At Spectrom* 27 (7):1131-1142.
14. Wimuktiwan P, Shioatana J, Siripinyanond A (2015) Investigation of silver nanoparticles and plasma protein association using flow field-flow fractionation coupled with inductively coupled plasma mass spectrometry (FIFFF-ICP-MS). *J Anal At Spectrom* 30 (1):245-253.
15. Ramos K, Ramos L, Camara C, Gomez-Gomez MM (2014) Characterization and quantification of silver nanoparticles in nutraceuticals and beverages by asymmetric flow field flow fractionation coupled with inductively coupled plasma mass spectrometry. *J Chromatogr* 1371:227-236.

16. Philippe A, Gangloff M, Rakcheev D, Schaumann GE (2014) Evaluation of hydrodynamic chromatography coupled with inductively coupled plasma mass spectrometry detector for analysis of colloids in environmental media - effects of colloid composition, coating and shape. *Analytical Methods* 6 (21):8722-8728.
17. Lewis DJ (2015) Hydrodynamic chromatography - inductively coupled plasma mass spectrometry, with post-column injection capability for simultaneous determination of nanoparticle size, mass concentration and particle number concentration (HDC-PCi-ICP-MS). *Analyst* 140 (5):1624-1628.
18. Soto-Alvaredo J, Montes-Bayon M, Bettmer J (2013) Speciation of Silver Nanoparticles and Silver(I) by Reversed-Phase Liquid Chromatography Coupled to ICPMS. *Anal Chem* 85 (3):1316-1321.
19. Franze B, Engelhard C (2014) Fast Separation, Characterization, and Speciation of Gold and Silver Nanoparticles and Their Ionic Counterparts with Micellar Electrokinetic Chromatography Coupled to ICP-MS. *Anal Chem* 86 (12):5713-5720.
20. Laborda F, Bolea E, Jimenez-Lamana J (2014) Single Particle Inductively Coupled Plasma Mass Spectrometry: A Powerful Tool for Nanoanalysis. *Anal Chem* 86 (5):2270-2278.
21. Yang Y, Long CL, Yang ZG, Li HP, Wang Q (2014) Characterization and Determination of Silver Nanoparticle Using Single Particle-Inductively Coupled Plasma-Mass Spectrometry. *Chin J Anal Chem* 42 (11):1553-1559.
22. Lee S, Bi XY, Reed RB, Ranville JF, Herckes P, Westerhoff P (2014) Nanoparticle Size Detection Limits by Single Particle ICP-MS for 40 Elements. *Environ Sci Technol* 48 (17):10291-10300.
23. Mitrano DM, Ranville JF, Bednar A, Kazor K, Hering AS, Higgins CP (2014) Tracking dissolution of silver nanoparticles at environmentally relevant concentrations in laboratory, natural, and processed waters using single particle ICP-MS (spICP-MS). *Environ-Sci Nano* 1 (3):248-259.
24. Furtado LM, Hoque ME, Mitrano DF, Ranville JF, Cheever B, Frost PC, Xenopoulos MA, Hintelmann H, Metcalfe CD (2014) The persistence and transformation of silver nanoparticles in littoral lake mesocosms monitored using various analytical techniques. *Environ Chem* 11 (4):419-430.
25. Mitrano DM, Leshner EK, Bednar A, Monserud J, Higgins CP, Ranville JF (2012) Detecting nanoparticulate silver using single-particle inductively coupled plasma-mass spectrometry. *Environ Toxicol Chem* 31 (1):115-121.
26. Peters RJB, Rivera ZH, van Bommel G, Marvin HJP, Weigel S, Bouwmeester H (2014) Development and validation of single particle ICP-MS for sizing and quantitative determination of nano-silver in chicken meat. *Anal Bioanal Chem* 406 (16):3875-3885.
27. Loeschner K, Navratilova J, Kobler C, Molhave K, Wagner S, von der Kammer F, Larsen EH (2013) Detection and characterization of silver nanoparticles in chicken meat by asymmetric flow field flow fractionation with detection by conventional or single particle ICP-MS. *Anal Bioanal Chem* 405 (25):8185-8195.
28. Pergantis SA, Jones-Lepp TL, Heithmar EM (2012) Hydrodynamic Chromatography Online with Single Particle-Inductively Coupled Plasma Mass Spectrometry for Ultratrace Detection of Metal-Containing Nanoparticles. *Anal Chem* 84 (15):6454-6462.
29. Grombe R, Allmaier G, Charoud-Got J, Dudkiewicz A, Emteborg H, Hofmann T, Larsen EH, Lehner A, Llinas M, Loeschner K, Molhave K, Peters RJ, Seghers J, Solans C, von der Kammer F, Wagner S, Weigel S, Linsinger TPJ (2015) Feasibility of the development of reference materials for the detection of Ag nanoparticles in food: neat dispersions and spiked chicken meat. *Accredit Qual Assur* 20 (1):3-16.

- 1
- 2
- 3 30. Liu JY, Murphy KE, MacCuspie RI, Winchester MR (2014) Capabilities of Single Particle
- 4 Inductively Coupled Plasma Mass Spectrometry for the Size Measurement of Nanoparticles: A
- 5 Case Study on Gold Nanoparticles. *Anal Chem* 86 (7):3405-3414.
- 6
- 7 31. Cornelis G, Hasselov M (2014) A signal deconvolution method to discriminate smaller
- 8 nanoparticles in single particle ICP-MS. *J Anal At Spectrom* 29 (1):134-144.
- 9
- 10 32. Rigo C, Ferroni L, Tocco I, Roman M, Munivrana I, Gardin C, Cairns W, Vindigni V, Azzena B,
- 11 Barbante C, Zavan B (2013) Active Silver Nanoparticles for Wound Healing. *Int J Mol Sci* 14
- 12 (3):4817-4840.
- 13
- 14 33. Roman M, Rigo C, Munivrana I, Vindigni V, Azzena B, Barbante C, Fenzi F, Guerriero P, Cairns
- 15 WRL (2013) Development and application of methods for the determination of silver in
- 16 polymeric dressings used for the care of burns. *Talanta* 115:94-103.
- 17
- 18 34. Solé VA, Papillon E, Cotte M, Walter P, Susini J (2007) A multiplatform code for the analysis of
- 19 energy-dispersive X-ray fluorescence spectra. *Spectrochim Acta B* 62 (1):63-68.
- 20
- 21 35. Ravel B, Newville M (2005) ATHENA, ARTEMIS, HEPHAESTUS: data analysis for X-ray absorption
- 22 spectroscopy using IFFFIT. *J Synchrotron Radiat* 12 (4):537-541.
- 23
- 24 36. Tuoriniemi J, Cornelis G, Hasselov M (2014) Improving the accuracy of single particle ICPMS
- 25 for measurement of size distributions and number concentrations of nanoparticles by
- 26 determining analyte partitioning during nebulisation. *J Anal At Spectrom* 29 (4):743-752.
- 27
- 28 37. Montano MD, Badiei HR, Bazargan S, Ranville JF (2014) Improvements in the detection and
- 29 characterization of engineered nanoparticles using spICP-MS with microsecond dwell times.
- 30 *Environ-Sci Nano* 1 (4):338-346.
- 31
- 32 38. Hineman A, Stephan C (2014) Effect of dwell time on single particle inductively coupled plasma
- 33 mass spectrometry data acquisition quality. *J Anal At Spectrom* 29 (7):1252-1257.
- 34
- 35 39. Pace HE, Rogers NJ, Jarolimek C, Coleman VA, Higgins CP, Ranville JF (2011) Determining
- 36 Transport Efficiency for the Purpose of Counting and Sizing Nanoparticles via Single Particle
- 37 Inductively Coupled Plasma Mass Spectrometry. *Anal Chem* 83 (24):9361-9369.
- 38
- 39 40. Cedervall T, Lynch I, Lindman S, Berggard T, Thulin E, Nilsson H, Dawson KA, Linse S (2007)
- 40 Understanding the nanoparticle-protein corona using methods to quantify exchange rates and
- 41 affinities of proteins for nanoparticles. *Proc Natl Acad Sci U S A* 104 (7):2050-2055.
- 42
- 43 41. Shannahan JH, Lai XY, Ke PC, Podila R, Brown JM, Witzmann FA (2013) Silver Nanoparticle
- 44 Protein Corona Composition in Cell Culture Media. *PLoS One* 8 (9).
- 45
- 46 42. Rigo C, Roman M, Munivrana I, Vindigni V, Azzena B, Barbante C, Cairns WRL (2012)
- 47 Characterization and evaluation of silver release from four different dressings used in burns
- 48 care. *Burns* 38 (8):1131-1142.
- 49
- 50 43. Adams NWH, Kramer JR (1999) Silver speciation in wastewater effluent, surface waters, and
- 51 pore waters. *Environ Toxicol Chem* 18 (12):2667-2673.
- 52
- 53 44. Larese FF, D'Agostin F, Crosera M, Adami G, Renzi N, Bovenzi M, Maina G (2009) Human skin
- 54 penetration of silver nanoparticles through intact and damaged skin. *Toxicology* 255 (1-2):33-
- 55 37.
- 56
- 57 45. Armitage SA, White MA, Wilson HK (1996) The determination of silver in whole blood and its
- 58 application to biological monitoring of occupationally exposed groups. *Ann Occup Hyg* 40
- 59 (3):331-338.
- 60
- 61
- 62 46. Wang XQ, Kempf M, Mott J, Chang HE, Francis R, Liu PY, Cuttle L, Olszowy H, Kravchuk O, Mill J,
- 63 Kimble RM (2009) Silver Absorption on Burns After the Application of Acticoat (TM): Data
- 64 From Pediatric Patients and a Porcine Burn Model. *J Burn Care Res* 30 (2):341-348.
- 65
- 66 47. Schneider L, Korber A, Grabbe S, Dissemmond J (2007) Influence of pH on wound-healing: a new
- 67 perspective for wound-therapy? *Arch Dermatol Res* 298 (9):413-420.

Table 1 Semiquantitative speciation of Ag in the dressing Acticoat Flex3™, 10 nm size AgNPs and ionic Ag incubated in solutions containing HSA or in whole human plasma for 2 h. Data were obtained by LCF of the μ XANES spectra; the AgGSH standard is representative of Ag-thiol bonds.

Experiment	Species	Molar fraction %
Ag ⁰ NPs 10 nm in plasma	Ag ⁰ foil	66
	Ag ⁰ NPs 10nm	28
	other	6
Ag ⁺ in plasma	AgCl	63
	other(x2)	37
Ag ⁰ NPs 10 nm in HSA	Ag ⁰ NPs 10nm	93
	AgGSH	7
Ag ⁺ in HSA	AgGSH	67
	other	33
Acticoat Flex3™	Ag ⁰ NPs 10nm	66
	Ag ⁰ foil	34
Acticoat Flex3™ in plasma	AgCl	59
	Ag ⁰ NPs 10nm	32
	AgGSH	10

Table 2 Main clinical information on the burnt adult patients treated with Acticoat Flex3™, and concentration of total Ag and dissolved Ag fraction in their whole blood.

	Patient A		Patient B	Patient C
Burn location	Torso + left arm		Torso	Torso + arms
Burned body surface, %	22		27	30
Degree	II		II	II
Dermabrasion	yes		yes	yes
Treatment duration, days	3	6	3	3
Total Ag in blood, ng mL ⁻¹	46.6	48.9	83.1	36.9
Total Ag in centrifugated blood, ng mL ⁻¹ (recovery %)	44.5 (96)	46.7 (96)	81.4 (98)	28.1 (76)
Dilution factor	100	100	250	75
Dissolved Ag in centrifugated blood, ng mL ⁻¹ (molar fraction %)	37.9 (85)	41.6 (89)	83.9 (103)	28.0 (100)

Table 3 Characterization of the AgNPs standards (mother suspensions) used throughout the study. Particles' diameter and geometry were measured by TEM on a minimum sample of 400 particles; for the z-potential $n = 5$.

Nominal size \pm SD (nm)	Measured diameter (nm):		Geometry:		z-potential (mV)
	Median (interquartile range)	Average \pm SD	Circularity \pm SD	Roundness \pm SD	
	Mode		Solidity \pm SD		
10 ± 4	8.6 (7.1 – 10.8)		0.90 ± 0.03		-46.4 ± 2.2
	9.2 ± 3.2		0.91 ± 0.06		
	7.2		0.95 ± 0.01		
20 ± 4	22.2 (20.7 – 23.5)		0.90 ± 0.02		-46.6 ± 2.0
	21.9 ± 2.4		0.91 ± 0.05		
	23.1		0.95 ± 0.01		
40 ± 4	40.7 (40.2 – 45.1)		0.89 ± 0.02		-45.3 ± 1.7
	42.4 ± 3.8		0.90 ± 0.05		
	43.5		0.96 ± 0.01		
60 ± 4	56.4 (50.6 – 59.7)		0.89 ± 0.02		-48.6 ± 1.2
	56.5 ± 4.5		0.89 ± 0.06		
	58.7		0.96 ± 0.01		
100 ± 4	98.7 (95.6 – 102.3)		0.88 ± 0.02		-53.2 ± 1.4
	99.0 ± 5.1		0.89 ± 0.05		
	98.7		0.95 ± 0.01		

Figure captions

Fig. 1 External calibrations applied to elaborate the HDC-spICP-MS chromatograms. a) 1st-99th interpercentile range of the normalized signal intensity relative to the average value calculated for dissolved Ag 500 pg mL⁻¹ within 2 s time windows, plotted against the corresponding average intensity. The range was adopted as the variable threshold for deconvolution of dissolved Ag and AgNPs signals. b) Calibration of the normalized signal intensity as a function of the mass of AgNPs standards with 20, 40, 60 and 100 nm nominal diameter (hypothesis of purely metallic spherical particles, n = 3). c) Calibration of the elution time as function of the diameter of AgNPs standards with 20, 40, 60 and 100 nm nominal diameter (n = 3). d) Calculation of the AgNPs detection efficiency as slope of the regression line, detected mass vs. injected mass (bilog scale). The injected standards were: 20 nm (5, 10, 20, 30, 40 pg), 40 nm (2.5, 5, 10, 20, 50 pg), 60 nm (10, 20, 50, 100, 200 pg) and 100 nm (25, 50, 100, 200, 500 pg). e) Calibration of the peak area for dissolved Ag (n = 3).

Fig. 2 3D contour plot chromatograms of AgNPs obtained for a mixture of 20, 40, 60 and 100 nm standards diluted in mobile phase (a, b) and the same mixture incubated for 2 h in plasma (c, d).

Fig. 3 a) Temporal variation of the molar fractions of AgNPs and dissolved Ag in plasma after incubation of a 100 nm standard from 2 to 24 h, average ± standard deviation, n = 3. b) Temporal variation of the mode of the AgNPs mass-derived distribution in the same incubated standard, average ± theoretical uncertainty, n = 3.

Fig. 4 3D contour plot chromatograms of AgNPs after incubation of the dressing Acticoat Flex3TM in plasma for 2 h.

Fig. 5 a) μXANES spectra of pure standards of Ag species; b) μXANES spectra of the intact dressing Acticoat Flex3TM, and AgNPs 10 nm and ionic Ag incubated in a solution containing HSA or in whole human plasma. The original spectra of the incubated standards are superimposed to their best fitting (dotted lines) obtained by LCF using the pure standards as the input variables. The fitting parameters (molar fractions) are reported in Table 1. AgGSH is representative of the Ag-thiol bounds.

Fig. 6 a) μXRF map of the distribution of Ag, Cl and S in the region surrounding a micrometric agglomerate of AgNPs released by Acticoat Flex3TM after 2 h incubation in plasma. Scale is linear in cps with independent full-scale values. b) μXANES map of Ag speciation in the same region. Scale is linear in cps with the same full-scale value for all species. AgGSH is representative of the Ag-thiol bounds.

Fig. 7 Deconvoluted chromatograms of dissolved Ag in whole blood of burnt patients obtained by HDC-spICP-MS. The blood was collected 3 days (patients A3, B and C) and 6 days (patient A6) after the application of the dressing Acticoat Flex3TM containing AgNPs. Each sample was differently diluted (see Table S-1) before injection to achieve a comparable concentration (~400 pg mL⁻¹).

Fig. 8 TEM images of the AgNPs standards (mother suspensions) used throughout the study; the nominal sizes are 10 (a), 20 (b), 40 (c), 60 (d) and 100 (e) nm

1
2
3 **Online Abstract Figure** Simplified scheme of the combined analytical approach adopted for
4 studying the chemical dynamics of AgNPs in human plasma/blood.
5
6
7
8
9
10
11
12
13
14
15
16
17
18
19
20
21
22
23
24
25
26
27
28
29
30
31
32
33
34
35
36
37
38
39
40
41
42
43
44
45
46
47
48
49
50
51
52
53
54
55
56
57
58
59
60

For Peer Review

Hydrodynamic chromatography coupled to single-particle ICP-MS for the simultaneous characterization of AgNPs and determination of dissolved Ag in human plasma and blood by of burnt patients
~~HDC- μ ICP-MS combined with μ XANES to elucidate the fate of AgNPs after topical administration to burnt patients~~

Marco Roman^{1,2*}, Chiara Rigo¹, Hiram Castillo-Michel³, Ivan Munivrana⁴, Vincenzo Vindigni⁴, Ivan Mičetić⁵, Federico Benetti⁵, Laura Manodori⁵, Warren R.L. Cairns²

¹ Ca' Foscari University of Venice, Department of Environmental Sciences, Informatics and Statistics (DAIS), Dorsoduro 2137, 30123 Venice, Italy

² Institute for the Dynamics of Environmental Processes (IDPA-CNR), Dorsoduro 2137, 30123 Venice, Italy

³ European Synchrotron Radiation Facility (ESRF), 71 avenue des Martyrs, 38000 Grenoble, France

⁴ Burns Center, Division of Plastic Surgery, University Hospital of Padua, Via Giustiniani 2, 35128 Padua, Italy

⁵ European Center for the Sustainable Impact of Nanotechnology (ECSIN), Viale Porta Adige 45, 45100 Rovigo, Italy

Corresponding author: Marco Roman

Ca' Foscari University of Venice, Department of Environmental Sciences, Informatics and Statistics (DAIS), Dorsoduro 2137, 30123 Venice, Italy

Phone: +0039 041 234 8545

Email: marco.roman@unive.it

Abstract

Silver nanoparticles (AgNPs) are increasingly used in medical devices as innovative antibacterial agents, but no data are currently available on their chemical transformations and fate *in vivo* in the human body, particularly on their potential to reach the circulatory system. To study the processes involving AgNPs in human plasma and blood, we developed a new analytical method for the simultaneous determination of dissolved Ag and the characterization of AgNPs in human plasma and blood, based on hydrodynamic chromatography (HDC) hyphenated to ICP-MS in single-particle detection mode, and combined with a innovative new algorithm was implemented to deconvolute the signals of dissolved Ag and AgNPs, and to extrapolate a multiparametric characterization of the particles for data treatment in the same chromatogram. From a single injection, the method provides the concentration of dissolved Ag and the distribution of AgNPs in terms of hydrodynamic diameter, mass-derived diameter, number and mass concentration. This analytical approach is robust and suitable to study quantitatively the dynamics and kinetics of AgNPs in complex biological fluids, included processes such as agglomeration, dissolution, and formation of proteins coronas. The method was applied to study the transformations of AgNPs standards and an AgNPs-coated dressing in human plasma, supported by μ XRF and μ XANES speciation analysis and imaging, and . The results showed that chlorides and protein thiols co-participate in the partial dissolution of AgNPs on an hourly time scale through complex dynamics driven by kinetic factors. The method was then applied to investigate for the first time the possible presence of AgNPs in the analysis of whole blood of samples collected from three burnt patients treated with the same AgNPs-coated dressing. Of the 30 to 80 ng mL⁻¹ of total Ag found in the blood, the dissolved fraction was not statistically different

1
2
3 | ~~from the total level of the metal, while NPs were not detected.~~ Together with our previous
4 studies, the results strongly support the hypothesis that the systemic mobilization of the metal
5 after topical administration of AgNPs is driven by their dissolution *in situ*.
6
7

8 **Keywords**

9 Silver nanoparticles; ~~Burns~~; Hydrodynamic chromatography; Single-particle ICP-MS; Synchrotron
10 radiation; Burns; Wound dressings
11
12
13
14
15
16
17
18
19
20
21
22
23
24
25
26
27
28
29
30
31
32
33
34
35
36
37
38
39
40
41
42
43
44
45
46
47
48
49
50
51
52
53
54
55
56
57
58
59
60

For Peer Review

Introduction

The multispectral antimicrobial effects of silver (Ag) are known and have been exploited since ancient times, but its use in consumer products and medical devices has proliferated considerably in recent years [1]. Ag-containing devices are widely used in hospitals as adjuvants in the treatment of pathologies where the control of bacterial infections is a key factor for a favourable prognosis [1,2]. The treatment of burns and chronic skin lesions is one of the most important applications because the local interruption of the blood flow make systemic infection prophylaxes little effective, and topical administration of Ag-based antimicrobials may therefore be decisive in preventing sepsis [2].

The reactivity of Ag in biological systems is mainly due to the ionic form Ag^+ , thanks to its ability to bind organic ligands [3]. In bacteria, such interactions allow the metal to bind to the cell wall, enter the cytoplasm, and interfere in key metabolic pathways [4]. However, the high reactivity of Ag^+ in biological systems may also lead to a rapid deactivation and clearance of the metal, mediated for example by complexation with serum proteins [5]. Engineered nanoparticles (NPs) provide innovative forms of Ag which can be specifically designed to modulate the release of ions from their surface in a gradual and highly controlled way [6]. Metallic AgNPs have the potential to persist sufficiently for mobilization within biological tissues, and exhibit enhanced affinity for cellular membranes, all of which favours their uptake and delivery to intracellular targets [7]. Several physico-chemical characteristics of AgNPs are determinant for their dynamics, including size/shape, surface charge and coating, as well as aggregation/agglomeration state. Many properties of the medium also affect their stability in biological systems, including the ionic strength, pH, pE, and composition of the organic matter [4]. Complex interactions among these properties of AgNPs and the surrounding media have been conjectured to regulate their transformations in environmental and biological systems [3], but the actual dynamics *in situ* and *in vivo* in human tissues remain currently unknown.

A key question is to establish whether AgNPs are able to remain intact for a sufficient length of time and space to reach the bloodstream and undergo systemic distribution. To address this question, adequate analytical tools to detect AgNPs and dissolved Ag in blood must be developed. Techniques such as transmission electron microscopy (TEM), scanning electron microscopy (SEM) and atomic force microscopy (AFM) enable size characterization of NPs at high resolution [8-10], but cannot provide statistically robust and quantitative data on complex biological fluids with a very low concentration of the metal. Dynamic and static light scattering (DLS and SLS) are widely used to characterize NPs suspensions, but are also inadequate for the analysis of polydisperse particles in complex biological matrices [11,12]. In addition, none of these techniques provides information on the dissolved fraction of a metal. A powerful technique for quantitative detection of metallic NPs is ICP-MS, as it is element-specific and highly sensitive, although it has to be coupled to a separation technique to gain a dimensional characterization. A variety of separation techniques, including flow-field-flow fractionation (FFF), hydrodynamic chromatography (HDC), reverse-phase (RP) high performance liquid chromatography (HPLC), ion mobility chromatography (IMC) and micellar electrokinetic chromatography (MEC), have been coupled to ICP-MS for the characterization of AgNPs in standard solutions, plasma and serum, nutraceuticals and a beverage [13-16,11,17,18]. However, all these separation techniques have limitations. Low recoveries are a critical issue in FFF, due to the complex interactions of AgNPs with the membrane, and dissolved ions cannot be detected [11]. RP-HPLC is able to separate AgNPs from ionic Ag, but with poor resolution and low reproducibility for complex biological matrices such as bovine serum [18]. HDC is a robust and versatile method for separating NPs even in complex and heavy matrices, but with poor resolving power. Dissolved ions could also be potentially determined by HDC-ICP-MS, but this

1
2
3 application has not yet been explored. MEC-ICP-MS could enable the size-dependent separation of
4 AgNPs and ionic Ag with a higher resolving power, but has only been tested on standards [19]. The
5 recent introduction of [the](#) single-particle (sp) acquisition mode in ICP-MS has allowed this
6 technique to detect NPs individually, providing quantitative information on their mass distribution
7 and number concentration in solutions [20]. A number of applications have been proposed for the
8 characterization of AgNPs in waters [21-25], but biological matrices remain virtually unexplored,
9 with the exception of enzymatically digested chicken meat [26]. However, spICP-MS does not
10 provide key data for the dynamics of AgNPs in complex systems, including the real diameter,
11 shape, composition, and aggregation/agglomeration of the particles, because only their metallic
12 mass can be revealed. The most promising strategy to obtain complete information on NPs in
13 complex media are spICP-MS hyphenated techniques, but only a few applications have been
14 proposed until now. Online coupling of asymmetric FFF (AF4) to spICP-MS has been explored to
15 study AgNPs in chicken meat [27], and so has HDC-spICP-MS for Ag, Au and polymeric NPs in
16 standards solutions and waters [28,16,12]. The determination of dissolved Ag in combination with
17 spICP-MS remains an analytical challenge. Off-line separation of the dissolved fraction by
18 ultrafiltration has been proposed [29,24], but simultaneous on-line methods would be preferable.
19 Statistical separation of the signals generated by AgNPs and dissolved Ag is possible in spICP-MS
20 by adopting a simple threshold value fixed on the standard deviation of the background
21 [12,25,21,30], or by applying a more complex algorithm based on polygaussian fitting of the
22 frequency distribution [31]. However, such strategies are not suitable for hyphenated techniques,
23 in which dissolved Ag itself generates a transient signal. Thus, the deconvolution of signals from
24 dissolved Ag and AgNPs in spICP-MS hyphenated techniques has not yet been attempted.

25
26 The goals of the present work were to set up and apply an analytical method based on HDC
27 hyphenated to spICP-MS for the simultaneous determination of dissolved Ag and the full
28 characterization of AgNPs in human plasma/blood based on an innovative signal deconvolution
29 strategy. An innovative approach combining our method with μ XRF imaging and μ XANES
30 speciation analysis was applied to study *in vitro* the transformations of AgNPs incubated in whole
31 human plasma, and to investigate for the first time the presence of AgNPs in the whole blood of
32 burnt patients treated by topical administration of AgNPs under real hospital conditions.

33 34 35 36 37 38 39 40 41 42 43 44 45 46 47 48 49 50 51 52 53 54 55 56 57 58 59 60

1. Experimental

Standards, reagents and samples

An Ag ICP-MS grade 1000 ng mL⁻¹ standard solution (certificated, NIST teachable) was obtained from Ultra Scientific (Bologna, Italy) and used to calibrate the total Ag measurements. Commercial standards of AgNPs purchased from Sigma-Aldrich were used for method development, calibrations and the incubation experiments. The standards consisted of monodisperse metallic NPs with nominal diameters of 10, 20, 40, 60 and 100 nm (provided uncertainty ± 4 nm), mass concentration 20 ± 0.5 μ g mL⁻¹, suspended in aqueous solution and stabilized with sodium citrate. The standards were characterized by TEM resulting in a size distribution compatible with the values provided by the manufacturer, and spherical shape. The z-potential of the mother dispersions was measured confirming their good stability (<-40 mV). Details on the experimental procedures for characterization of the standards, representative TEM images and a summary of their size/shape parameters and z-potential can be found in the appendix. The measured size of the standards was used for all calculations, but for simplicity, we refer to their nominal diameter throughout this paper. The exact mass concentration as total Ag of the mother dispersions was also measured by ICP-MS, and number concentration was calculated based on the experimental mode of the size distribution.

1
2
3 The commercial dressing Acticoat Flex3™ (Smith & Nephew) was used for the *in vitro* incubations
4 and the *in vivo* treatment of burnt patients as reported elsewhere [32]. The mobile phase for
5 chromatography was prepared using sodium dodecyl sulphate (SDS), HNa_2PO_4 dihydrate and
6 IGEPAL® CA-630 nonionic detergent in the following concentrations: SDS 0.05 % v/v, HNa_2PO_4
7 0.002 M and IGEPAL 0.1 % v/v at pH 7.4. A water solution containing tetramethylammonium
8 hydroxide (TMAH) 0.1 % v/v, NH_4OH 2.8 % w/w and Triton™ X-100 0.1 % v/v was used to dilute
9 20-fold the whole blood for total Ag determination by ICP-MS. L-glutathione reduced (GSH) and
10 human serum albumin (HSA) lyophilized powders were used for incubation experiments. All
11 incubations were carried out in a normal laboratory environment at 37 °C in a thermostated bath,
12 under constant gentle shaking in the dark. The preparation steps for standards and samples were
13 carried out in a class 1000 clean room environment under a class 100 laminar flow bench.

14
15 Whole human plasma for incubations and control whole blood were provided by distinct
16 volunteers and were collected at the University Hospital of Padua. Four samples of whole blood
17 were provided by the bio-bank of the same Hospital, and were collected from three adult patients
18 treated in the same Hospital, at the Burns Center, following the current protocols without any
19 additional invasive procedure. The patients did not present any pathology other than the burn. All
20 samples were collected and stored in agreement with the guidelines of the University Hospital of
21 Padua and informed consent of the patients was obtained according to the Helsinki Declaration.
22 The blood was collected in purple-tip vials (K2-3EDTA) in order to prevent coagulation, was
23 immediately frozen to lyse the red blood cells, and was stored frozen until analysis.

24 Instrumentation

25
26 The chromatographic system consisted of an Agilent Technologies (Tokyo, Japan) 1200 series HPLC
27 pump fitted with an HDC 5-300 Type-1 column (linearity range from 5 to 300 nm) from the same
28 supplier. Sample injections were performed manually using a 100 μL loop and an inert Rheodyne
29 injection valve. The elution was performed in isocratic mode at a flow rate of 1.0 mL min^{-1} . An ICP-
30 MS detector model 7500cx from Agilent Technologies was coupled on-line to the chromatographic
31 system by using a polypro nebulizer mounted on a double-pass Scott spray chamber thermostated
32 at 2°C. The instrument operated at 1500 W RF power with a carrier gas flow rate of 1.1 mL min^{-1}
33 and make up gas flow rate of 0.1 mL min^{-1} . The lens voltages were tuned daily for best sensitivity
34 using a 1 ng mL^{-1} solution of Ag. In order to minimize the matrix effects, robust plasma conditions
35 were achieved by-keeping oxides and double charges rates below 2 % based on the response of a
36 Ce 1 ng mL^{-1} solution, and using 8 mm of sample depth. Acquisition was carried out by monitoring
37 both the isotopes of Ag (m/z 107 and 109) with a dwell time of 5 ms. Automatic correction for the
38 dead time was adopted, the parameter was estimated as reported elsewhere [33]. A settling time
39 of 2 ms was automatically selected by the instrument and was taken into account to correct the
40 calibration of NPs number concentration, as reported below.

41
42 Synchrotron radiation μXRF and Ag L_{III} -edge μXANES measurements were performed using the
43 scanning transmission X-ray microscope of beamline ID21 at the European Synchrotron Radiation
44 Facility (ESRF, Grenoble, France). Details on standards/sample preparation, instrumental
45 parameters and data elaboration for μXRF and μXANES are provided as supporting information.

46 Data elaboration

47
48 Data treatment for HDC-splCP-MS was carried out by using a home-made program written in
49 Fortran language and run using the compiler Compaq Visual Fortran (Compaq Computer
50 Corporation). The program reads the ICP-MS raw data file directly and provides a number of
51 output files including overall statistics and matrices. The latter were directly imported in Surfer 11
52 (Golden Software) for graphical elaboration of the contour plots (3D chromatograms). Excel

spreadsheets (Microsoft), OriginPro 8.5 (OriginLab) and Statistica 10 (StatSoft) were used for additional calculations and graphical elaboration. PyMca [34] and Athena [35] software were used to elaborate the μ XRF and μ XANES data.

2. Results and discussion

2.1. Implementation of data analysis

2.1.1. *Dwell time and data pre-processing*

The limit of detection (LOD) in spICP-MS has two possible interpretations: as the lowest detectable particle size (LOD_S^{NP}) and the lowest detectable particle number (LOD_N^{NP}). Measuring simultaneously the dissolved Ag introduces also a third definition, which is the lowest detectable concentration of this fraction (LOD_C^D). The choice of the dwell time is the key to determine ~~the limit of detection all these (LOD) parameters in samples where both NPs and dissolved Ag are present,~~ and the overall statistical reliability of the results in spICP-MS. Individual NPs in ICP-MS generate transient signals with a temporal width of 0.3-0.5 ms [36]. Recent instrumentation allows setting the dwell time within the μ s range, so that single events can be described by multiple data points. This results in a significant reduction of the background, a decreased LOD_S^{NP} ~~dimensional LOD for the NPs~~ and an improved range of number concentration [37]. However, the same increase in the signal-to-background ratio is expected to make more difficult the determination of the dissolved Ag by statistical deconvolution within the same analysis, increasing the LOD_C^D . Moreover, with μ s dwell times, the probability to observe split of events between adjacent time windows must be taken into account [30], and the electronic and computational load due to data size can be potentially problematic when applied to hyphenated techniques, where the acquisition lasts for tens of minutes. Conversely, conventional ms dwell time leads to higher LOD_S^{NP} ~~LOD for the mass derived diameter~~ and requires higher dilution of the samples to avoid detecting multiple events within the same time window [30], but it is more suited for performing the simultaneous determination of dissolved Ag and using hyphenated instrumental approaches. According to other authors, a dwell time in the range of 3-5 ms is adequate to achieve good quality data in our context [38]. The minimum dwell time that can be set on our instrument for the acquisition of a single m/z is 10 ms, but a dwell time of 5 ms can be chosen by monitoring both masses of Ag. This required a data pre-processing step for normalization of the two signals to the relative natural abundance of each respective isotope, before merging them into a single chromatogram. Given the proximity of the two abundances (0.518 For ^{107}Ag and 0.482 for ^{109}Ag), the difference in signal intensity for the two masses is negligible at low counting rates, but was nevertheless taken into account when applying the threshold in the following deconvolution step. In addition, the acquisition of two masses introduces a settling time, which slightly affects the number of detected particles (see section 2.1.4.).

2.1.2. *Deconvolution of the signals*

The expected forms of dissolved Ag in plasma (protein complexes) have hydrodynamic diameters smaller than the LOD_S^{NP} ~~LOD of mass derived diameter for NPs,~~ (see section 2.1.4.), and close to the lower limit of separation range. Given also the poor resolving power of HDC, their peak cannot be chromatographically ~~resolved~~ from those of ~ 20 nm particles, thus making deconvolution a necessary operation. In this work, the statistical deconvolution of the signals from dissolved Ag species and AgNPs was based on a nonparametric statistical test applied to each data point of the chromatogram as it was sequentially scanned. The intensity value of each point was compared to that of its two adjacent neighbours, and their difference was calculated. If at least one of the two

differences overcame a threshold value given by the maximum expected difference between any data generated by dissolved Ag, the hypothesis of the point being associated to dissolved forms was rejected. For each pair of points to be compared, the relative threshold value was specifically calculated as a negative exponential function of the lower of the two intensities. The function was externally calibrated on the chromatogram of a single standard of dissolved Ag with a relatively high concentration (500 pg mL⁻¹) using the following procedure. The chromatogram was divided into consecutive windows of 2 s width, in which the signal was assumed to be stationary. For each window, the empirical distribution of the data was calculated to extract the 1st-to-99th interpercentile range. The range was plotted against the average value within the same window as shown in Fig. 1a. The interpercentile range can be interpreted as the maximum difference in signal intensity between two data points generated by dissolved Ag at a 98 % confidence level, and was adopted here as the threshold value to discriminate the signals. The vector of points for which the hypothesis of being generated by dissolved Ag was rejected, constituted the NPs extracted chromatogram.

2.1.3. Elaboration of the 3D NPs raw chromatogram

The NPs chromatogram was firstly treated by converting the normalized signal intensities into their cube square. This step was necessary to obtain final chromatograms in which the mass-derived diameter is represented on a scale with uniform resolution. In a second step, the dimensions of elution time and normalized signal intensity were gridded into windows of selected width according to the procedure proposed by Pergantis et al. [28]. The width of the intensity windows was fixed at 0.6266 normalized counts^{1/3}, resulting in a resolution of 6.5 nm for the mass-derived diameter after calibration. The width of the elution time windows was fixed at 5 s in order to contain 714 data points to guarantee statistical representativity. After gridding, the number of events detected within each window was counted, and a raw 3D chromatogram was yielded as a 3-columns matrix consisting of the central values of the elution time (x-axis) and the normalized events' intensity (y-axis), and the number of detected events (z-axis) for each window.

2.1.4. Calibrations and elaboration of the 3D NPs final chromatograms

Besides the threshold function, other external calibrations based on the injection of monodisperse NPs standards were necessary to convert the normalized signal intensity into mass-derived diameter, and the elution time into hydrodynamic diameter. Standard suspensions with a 20, 40, 60 and 100 nm nominal size and variable concentration were injected to calibrate these two parameters as done by Pergantis et. al. [28]. For each standard, the mode of the 3D raw chromatogram provided the data to be included in the calibration curves, which are shown in Fig. 1b,c. A LOD₅^{NP} of 16 nm was calculated as 3 times the standard error of the intercept of the mass calibration curve. This value is in agreement with the range of those estimated by other authors both theoretically and experimentally (in water samples) using spICP-MS [22]. The extrapolation of the number concentration of AgNPs in a sample required estimating separately their ~~detection-transport efficiency of NPs through the nebulization system, which corresponds to their transport efficiency corrected for the settling time.~~ Adapting the formula by According to Pace et al. [39], the overall number of detected particles n_r of radius r , using the hypothesis of purely metallic and spherical particles, can be expressed as:

$$n_r = \eta \cdot \frac{c_r^m}{\frac{4}{3}\pi r^3 \rho} \cdot v \cdot \frac{t_i}{t_s + t_i} \quad \text{eq.1}$$

where η is the transport efficiency (independent by the radius), c_r^m is the mass concentration of the NPs (pg mL⁻¹), v is the injection volume (mL), and ρ is the density of Ag in pg nm⁻³ = 1.049 · 10⁻⁸.

~~t_i is the integration time and t_s is the settling time.~~ The transport efficiency can be estimated by analyzing a series of standards of any radius at different known mass concentrations, calculated as the slope of the regression line in eq. 1. However, one should note that even if approximately monodisperse, a standard suspension still has a characteristic size distribution which may be not perfectly symmetric, particularly for the size ranges close to the LOD_5^{NP} , so that simple counting the overall number of detected particles would introduce a bias. In order to overcome this potential problem, we used the calibration of mass-derived diameter to convert the number of detected particles into a mass for each window of the raw chromatogram. Summing the mass of all windows provided the total detected mass of Ag, to be used in place of n_r for efficiency estimation. The method was tested on four nominal particles sizes, as shown in Fig. 1d. Consistently with the independence of η from the particles' size, an average value of $1.78 \pm 0.07\%$ was obtained for the four calibrations. If a minimum number of 3 detected particles is arbitrarily adopted as the statistical threshold to verify their presence, taking into account the transport efficiency, settling time and injection volume, a LOD_N^{NP} of ~ 2300 particles mL^{-1} is achieved. This threshold can be indifferently adopted for all particles or for specific size classes, which is very close to that ($\sim 1.7\%$) obtained by Pergantis et al. [28] using the number of detected gold NPs with 60 nm size, and a V-groove nebulizer. Finally, a calibration was also required for the dissolved Ag fraction by injecting standards of ionic Ag with variable concentration as shown in Fig. 1e, obtaining a LOD_C^D of 13 $pg\ mL^{-1}$.

All calibrations reported above allowed to convert the data of the 3D NPs raw chromatogram for each sample into a final chromatogram representing the experimental distribution of NPs in terms of number concentration or mass concentration depending on the hydrodynamic diameter and mass-derived diameter.

2.2. Stability of the AgNPs in the mother standards and in mobile phase.

The mother citrate-stabilized dispersions were stored at $4^\circ C$ and no significant changes in their size distribution were noticed after more than 1 year (as observed by TEM). In addition, no peaks of dissolved Ag were detected by HDC-ICP-MS when injecting single standards freshly diluted in mobile phase for calibration within the same time span. The temporal stability of AgNPs standards in the mobile phase below the $ng\ mL^{-1}$ level was also checked. Despite the appearance of small peaks of dissolved Ag was observed after leaving the vials exposed to light and room temperature up to 24 h, the corresponding concentration was below the LOD_C^D for all particle sizes. Nevertheless, in order to avoid any potential alteration of the dynamics of AgNPs due to interaction with the mobile phase, all standards for calibration were always prepared freshly from the mother dispersion and immediately injected, all samples were analysed immediately after preparation, and replicates were obtained from independent preparations rather than from repeated injections.

2.3. Dynamics of AgNPs incubated in human plasma

The developed method was used to study the dynamics of AgNPs in human plasma. Standards with nominal diameters of 20, 40, 60 and 100 nm were mixed in whole plasma at concentrations of 10, 16, 37 and $100\ ng\ mL^{-1}$, respectively, sonicated for 1 min and then incubated for 2 h. After incubation, the sample was diluted 20-fold in the mobile phase and directly injected without further sonication. A control sample was prepared by diluting the AgNPs mixture in the mobile phase at the same final concentration, followed by sonication for 1 min, and direct injection. Fig. 2 shows the final 3D chromatograms obtained for the control and plasma incubated mixtures. A number of significant changes were observed in the distributions of NPs after 2 h of incubation in plasma: i) a slight general decrease in the mass-derived diameter; ii) a significant decrease in the

number and mass concentration of the NPs; iii) a generalized shift in the distribution towards the higher hydrodynamic diameters of 10-20 nm. While the first two effects can be ascribed to a partial dissolution of the NPs, the increased hydrodynamic diameter is compatible with two possible phenomena: agglomeration of NPs and the formation of a protein corona onto their surface. The agglomeration of uncapped NPs is a feasible process in plasma, particularly due to the relatively high ionic strength of the medium [3]. We did not observe the appearance of new modes in the mass-derived diameter corresponding to multiples of the nominal diameters of 40, 60 and 100 nm. However, agglomeration effects cannot be excluded for the 20 nm particles due to the theoretical superimposition of the multiples of their mass on the modes of the other standards. Conversely, the formation of a proteins corona is a plausible generalized process, particularly due to the interaction of thiol groups in amino acids with the charged surface of AgNPs in a medium with a high ionic strength [40,41].

In order depict the temporal dependence of the dynamics of AgNPs in human plasma, the standard suspension with a 100 nm size was selected for further incubation experiments. An aliquot of the mother monodisperse suspension ($20 \mu\text{g mL}^{-1}$) was sonicated for 1 min, then mixed 1:1 with plasma and incubated for 24 h. At time steps of 2, 4, 6, 8, 16 and 24 h, aliquots of the solution were collected, diluted 10,000-fold in the mobile phase, and analyzed immediately. Fig. 3a shows that the dissolution of AgNPs is not linearly time-dependent on an hourly scale in a closed system. The most significant change was observed between the 4 and 8 h incubations, with a decrease in the molar fraction of Ag present in the original form of NPs, corresponding to the appearance and increase of the dissolved fraction. Between 16 and 24 h the molar fractions seem to reach equilibrium. The precision of detection efficiency ($\sim 4\%$ of relative error, see paragraph 2.1.), which affects the estimated number concentration, is the dominant source of uncertainty for AgNPs molar fraction. The calibration of dissolved Ag is more reproducible because the relative error of the slope of its calibration curve (Fig. 1e) is 1%. The mass-derived diameter of the particles exhibits a substantial linear decrease from 100 to 80 nm in 24 h (Fig. 3b), confirming the partial dissolution of the individual particles. In this case, the standard deviation among replicates is zero because their differences are smaller than the width of the signal intensity windows adopted for gridding (see paragraph 2.1.3.). Thus, for each estimated diameter d , the width of the gridding windows $\pm 6.5/d\%$ can be considered as the maximum theoretical uncertainty, and was taken to represent the whiskers in Fig. 3b.

Speciation analyses by μXANES were carried out on analogously incubated samples. Standards of AgNPs with a 10 nm size ($20 \mu\text{g mL}^{-1}$) and ionic Ag solution (nitrate, $10 \mu\text{g mL}^{-1}$ as Ag) were incubated in a water solution containing HSA ($\sim 0.5 \text{ mg mL}^{-1}$) and in whole plasma. After 2 h a drop of each solution was freeze-dried between Ultralene[®] windows and was directly analyzed by μXANES . Representative spectra for each of the incubated standards and pure species of Ag, as shown in Fig. 4a-b, allowed us to identify the chemical forms of Ag after incubation and their relative molar fractions estimated by linear combination fitting (LCF), as reported in Table 1. The μXANES analysis showed that after 2 h of incubation in HSA the Ag^+ ions were mostly complexed by thiols (represented by the Ag-GSH bound). Conversely, AgNPs remained intact almost quantitatively, even if Ag-thiols were also detectable. This confirms that the formation of a protein corona on the surface of AgNPs has a major inhibiting effect on their dissolution in the short term. Differently, in whole plasma, the early dynamics of Ag were dominated by chlorides, with formation of insoluble AgCl from free Ag^+ , and significant agglomeration of the AgNPs, as marked by the high weight of the metallic Ag foil spectrum obtained by LCF.

2.4. Dynamics of AgNPs agglomerates released from a dressing incubated in human plasma

1
2
3 The 2 h incubation experiment in whole plasma was carried out also by using the intact dressing
4 Acticoat Flex3™. The dressing consists of a net of polyethylene fibers, individually and uniformly
5 coated with a layer of uncapped AgNPs of 10 nm size; other characteristics of the product can be
6 found elsewhere [33]. Previous experiments showed that the dressing releases AgNPs as
7 agglomerates with widely variable size *in vitro* in human serum substitute [42], and agglomerates
8 were also detected in the fibroblasts of burnt patients after 7 days of treatment [32]. In this
9 experiment, 2.45 mg of the dressing (0.32 mg as Ag) were dipped into 1 mL of whole plasma and
10 sonicated for 10 min to accelerate the release of AgNPs as individual particles or small
11 agglomerates. After 2 h of incubation, the plasma was centrifuged at 3000 rpm for 10 min in order
12 to remove the fibers, cloth debris and micrometric agglomerates of AgNPs, then an aliquot was
13 diluted 100-fold in the mobile phase and directly injected into the chromatographic system. The
14 3D chromatograms in Fig. 5a-b show a few particles with size >16 nm, corresponding to small
15 agglomerates of 2-5 NPs with 10 nm size. Significantly higher hydrodynamic diameters, with
16 respect to the mass-derived diameter, were also observed. The latter effect supports the
17 hypothesis that the observed particles are small (non-spherical) agglomerates, and is also
18 compatible with additional proteins capping effects. The dissolved Ag fraction resulted lower than
19 the $LOD_{LOD_C}^D$.

20
21
22
23 A 20 μ L aliquot of the same sample after incubation was collected before centrifugation, was
24 freeze-dried and analyzed by μ XRF and μ XANES. Preliminary μ XRF mapping of the sample allowed
25 us to detect a number of micrometric agglomerates of AgNPs or fragments of the dressing. A
26 region surrounding one of the particles was selected, and the distribution of Ag, Cl and S was
27 mapped as shown in Fig. 6a. A characteristic non-uniform accumulation of Cl was observed at the
28 border of the Ag particle, while S was uniformly distributed in the surrounding medium. μ XANES
29 spectra were collected in the same region for each pixel to be individually elaborated by LCF
30 in order to extract a coarse estimation of the molar fraction of the three main expected species:
31 intact AgNPs, AgCl and Ag-thiols. The resulting μ XANES map is shown in Fig. 6b. Although total Ag
32 and Cl presented widely different distributions, a relatively uniform distribution of the Ag species
33 was observed, consistent with the participation of the whole surface of the AgNPs agglomerates in
34 the chemical dynamics of the metal. The average molar distribution of the species within the
35 entire region was 49 % AgCl, 22 % AgNPs and 20 % Ag-thiols (9 % unidentified species). The overall
36 distribution was also estimated by firstly merging all the spectra within the region, and then
37 performing the LCF on the pooled spectrum. This procedure allowed us to weight the contribution
38 of each pixel on the base of the total Ag level, and provided the values: 53 % AgCl, 31 % AgNPs and
39 15 % Ag-thiols. Compatibly with Fig. 6b, the slight variations with respect to the previous
40 estimation are consistent with a major localization of AgCl and AgNPs in the regions with elevated
41 Ag level, while Ag-thiols are mainly present in the peripheral areas. The assignment of previously
42 unidentified species could also have affected the latter values. The co-presence and relative
43 proportion of the three species reveal that the dynamics of AgNPs in plasma involve integrated
44 and complex processes. Free Ag ions are expected to be a negligible fraction in biological systems
45 due to the high formation constant for chloride and thiol bonds [43,3], so that dissolution and
46 formation of complexes may take place directly on the surface of the AgNPs as an integrated
47 process. Properties of the medium such as its general composition, concentration of chloride and
48 pH, and kinetics of complexation influence the dynamics. Although protein thiols should be
49 thermodynamically favoured for Ag binding in plasma with respect to chlorides [6,3], our data
50 support the hypothesis that the latter have a kinetic advantage when interacting with Ag ions
51 directly on the charged surface of the bare NPs, leading to an early effect of partial dissolution,
52 and possibly agglomeration of the smallest NPs. Still, protein thiols may co-participate to these
53 dynamics by enclosing the particles and superficial chlorides, inhibiting further interactions with
54
55
56
57
58
59
60

1
2
3 the medium, the removal of AgCl from the surface and further agglomeration effects. Given the
4 affinity of thiols for Ag, subsequent displacement of the metal from the chlorides is likely, resulting
5 in its final mobilization. In agreement with Liu et al. [3], thiols binding appears to be the limiting
6 process in regulating the dissolution of AgNPs in plasma, and the mediator for systemic
7 distribution of the metal, but our findings suggest that kinetic factors play a crucial role in this
8 complex dynamics.
9

10 11 **2.5. Whole blood from burnt patients treated with a AgNPs-containing dressing**

12
13 In addition to the temporal dynamics of the chemical transformations of AgNPs, the particles
14 could also undergo simultaneous mobilization through the tissues, with consequent change in the
15 properties of the surrounding medium. The formation of a proteins corona is probably the main
16 favouring factor for the cellular uptake on AgNPs [41], which has been observed in human skin
17 both *in vitro* and *in vivo* in burnt patients [32]. However, the few available experimental data
18 suggest that the metal has a poor capability to penetrate the skin in depth, even if penetration
19 may be enhanced in damaged tissue [32,44].
20

21
22 In order to evaluate the actual potential of AgNPs to reach the bloodstream before dissolution, we
23 used HDC-spICP-MS to analyze four whole blood samples collected from three **adult** patients (A-C)
24 treated for mid-thickness skin burns with a single application of the dressing. The main clinical
25 information is summarized in Table 42. The patients had a comparable % of burned body surface,
26 which represents the wound area exposed to AgNPs. Three blood samples were collected from
27 distinct patients 3 days after the application ~~of the dressing~~; and an additional sample was
28 collected from patient A after 6 days of treatment. Compatibly with our previous estimations that
29 the dose of Ag released by the dressing into the patient's tissues *in vivo* would be elevated [33], a
30 significant level of total circulating Ag was observed in all patients after 3 days of application of the
31 dressing (Table 2). The values ranged between ~30 to 80 ng mL⁻¹ and were more than 2 orders of
32 magnitude higher than the baseline level in an unexposed population [45], and slightly lower than
33 those observed in the serum of paediatric burnt patients treated with the same dressing (average
34 114 ng mL⁻¹) [46]. Differently from the latter cited work, we did not observe any apparent
35 correlation between blood Ag and the percentage of burnt body area, and just a slight increase in
36 Ag was noticed after 3 additional days of application for patient A.
37

38
39 An aliquot of the blood was then centrifuged at 3000 rpm for 10 min to remove the cell debris in
40 order to avoid clogging the chromatographic system. The supernatant was recovered and analyzed
41 for total Ag. The average recovery of total Ag after centrifugation was ≥ 96 % for all samples
42 except patient C (76 %), and a minimal loss of Ag due to co-precipitation was therefore assumed
43 for most cases. The possibly co-precipitated Ag can be ascribed to its association to cellular debris
44 and large biomolecules whose size exceeds the effective separation range of the HDC system.
45 Based on the total concentration of Ag, the centrifuged samples were diluted in the mobile phase
46 according to specific dilution factors (see Table 2), optimized to obtain the same final
47 concentration of ~400 pg mL⁻¹ of Ag. This target value was selected from preliminary tests as the
48 optimum concentration for detecting a significant number of AgNPs with a mass-derived size close
49 to the $LOD_S^{NP} \sim LOD$ under the hypothesis that they were present as a significant molar fraction of Ag
50 (> 10 %).
51

52
53 We did not detect any significant event associated to AgNPs agglomerates >16 nm in the four
54 blood samples (chromatograms are not shown). Conversely, from the chromatograms of dissolved
55 Ag shown in Fig. 7, an average molar fraction of 94 ± 9 % was estimated for the dissolved species
56 (see Table 2), which is not statistically different from the total level of the metal.
57
58
59
60

1
2
3 Considering that: i) our previous studies have shown that in burnt patients treated with Acticoat
4 Flex3™, AgNPs are released as agglomerates and maintain this form even in the tissue; ii) a poor
5 dermal penetration of PVP-coated AgNPs, restricted to small (<30 nm) particles in damaged skin,
6 was observed *in vitro* [44]; and iii) we documented here that small AgNPs exhibit both
7 agglomeration and partial dissolution effects at an hourly time scale in plasma; the results of blood
8 analysis strongly support the hypothesis that the systemic mobilization of Ag is driven by the *in*
9 *situ* dissolution of NPs in the skin. The first medium entering in contact with the AgNPs released by
10 the dressing onto the wound bed is the exudate, whose composition is similar to the serum. This
11 medium is the major candidate to host the *in situ* transformations of AgNPs, where dissolution
12 may be also enhanced by the lower pH (5.7), typical of the inflammatory phase in wounds [47]. It
13 is also likely that the reduced blood circulation in burns further inhibits the dispersion of AgNPs.
14 However, let us keep in mind that the specific local characteristics of the wound may dramatically
15 affect the release of AgNPs from the dressing and the composition/production/turnover of the
16 exudate. This can lead to significantly different AgNPs dynamics at a local level, resulting in the
17 possible penetration of agglomerates into the shallow tissue layers. Photochemical reduction of
18 Ag complexes with formation of secondary Ag/S/Se particles can also occur in the skin [3]. We
19 previously observed a few electron-dense particles in skin biopsies after application of the
20 dressing, which are potentially representative of photoprecipitation [32]. However, this
21 phenomenon appears to be limited to the most severe lesions, which require long-term
22 treatments and replacement of the dressing, leading to exposure to light and an increased Ag
23 dose.
24
25
26
27
28

29 3. Conclusion

30
31 The exponentially growing market of consumer and medical products containing AgNPs has raised
32 the urgent need for regulatory standards targeted at health and safety. Developing adequate
33 analytical methods to achieve detection and characterization of AgNPs and their ionic counterpart
34 in biological media is the key requisite to support regulatory requirements with robust scientific
35 evidence.
36

37 -An innovative method is proposed here for the simultaneous determination of dissolved Ag and
38 the characterization of AgNPs in human plasma and blood. By coupling HDC separation, spICP-MS
39 detection and a dedicated algorithm for data elaboration, comprehensive information on the
40 chemical state of the Ag⁺/AgNPs system can be retrieved in ~~one~~ single analytical run. While HDC
41 separates the NPs based on their hydrodynamic diameter and spICP-MS provides information on
42 their mass distribution, both techniques have the potential to discriminate physically and
43 statistically (respectively) the signal of NPs from that of dissolved Ag, but this advantage was not
44 exploited before. We combined the two techniques and a home-made software based on a new
45 algorithm able to process the raw ICP-MS chromatogram for deconvoluting the signal of dissolved
46 Ag from that of AgNPs. From a single injection, the method provides the chromatogram and
47 concentration of dissolved Ag; the distribution of NPs in terms of hydrodynamic diameter, mass-
48 derived diameter, size-dependent number of detected NPs; the total number concentration and
49 size-dependent mass concentration of the NPs. A variety of 3D chromatograms can be obtained
50 from the results to achieve a comprehensive characterization of AgNPs.
51

52 The method is robust when applied to heavy matrices such as plasma and blood, and in principle
53 can be extended to other biological media and to other metallic NPs. The algorithm in particular is
54 suitable for the deconvolution and determination of particulate and dissolved fractions
55 independently by the element, or just for the removal of non-stationary background in any
56 separation technique coupled to spICP-MS.
57
58
59
60

1
2
3 | Combining the method with ~~other techniques, such as~~ μ XANES speciation and imaging, provides
4 an integrated approach which opens the way to elucidate the dynamics of AgNPs in biological
5 fluids or extracts *in vivo* under realistic conditions (real human subjects, real administered doses).

6 | -We applied this strategy to study the behaviour of AgNPs standards and of an AgNPs-coated
7 dressing incubated in human plasma, and to investigate for the first time the capability of AgNPs
8 to reach the systemic circulation after topical application to burnt patients.

9
10 The results showed that partial dissolution of uncoated AgNPs takes place in plasma on an hourly
11 time scale with nonlinear dynamics in a closed system. Chlorides and protein thiols co-participate
12 in the process through complex temporal and spatial mechanisms, forced by kinetic factors. The
13 early dynamics and dissolution of AgNPs are dominated by interaction with chlorides directly on
14 their surface. Formation of a protein corona takes place in the meantime, resulting in the
15 inhibition of further reactions with the medium, slower displacement of Ag from chlorides and
16 final mobilization of the metal. As a whole, thiols binding is proposed as the main regulator of
17 AgNPs dissolution in plasma and of the systemic distribution of the metal. The analysis of whole
18 blood from burnt patients suggested that the dynamics of AgNPs dissolution after topical
19 administration takes place mainly *in situ*, most probably in the exudate, so that their potential to
20 undergo systemic distribution in the intact form is minimal. Further studies are currently in
21 progress to investigate the chemical speciation of Ag directly in wound tissues.

22 23 24 25 **Acknowledgments**

26
27
28 The authors are grateful to the Italian Ministry of Education, University and Research for financial
29 support through the project MIUR-FIRB number RBFRO8M6W8. The European Synchrotron
30 Radiation Facility is acknowledged for provision of beamtime at ID21. ELGA LabWater is
31 acknowledged for providing the PURELAB Option-Q and Ultra Analytic systems, which produced
32 the ultra-pure water used in these experiments. Francesca Benetello and Bruno Pavoni from Ca'
33 Foscari University of Venice are acknowledged for the lyophilisation of standards and samples.

34
35
36 **Disclaimer:** The authors declare that they have no conflict of interest.

37 38 **Appendix**

39 40 41 **Characterization of the commercial AgNPs standards dispersions**

42
43 The morphological characterization of the mother AgNPs standard dispersions was carried out by
44 TEM using a Tecnai 12 G² instrument (FEI, USA). For the analysis, a 3 μ L drop of each dispersion
45 was deposited on a support Formvar/Carbon on 200 mesh thick grid, let dry at room temperature
46 and directly analysed. The images were acquired at 120 kV high voltage and using tungsten
47 filament, twin optics and an Olympus side-mounted camera. The software ImageJ (National
48 Institutes of Health, USA) was used for particles' counting and shape characterization.
49 Representative TEM images of the standard NPs and a summary of their size/shape parameters
50 are shown in Fig. 8 and reported in Table 3, respectively.

51
52 The z-potential was measured by using a Zetasizer Nano (Malvern, UK) at 24°C in DTS1070 cells
53 pre-washed with a citrate 60 μ g mL⁻¹ water solution. For the analysis, each standard suspension
54 was sonicated for 5 min, equilibrated for 120 s in the cell, and 5 replicate measurements of 10 to
55 100 readings were acquired. The z-potential of the standard NPs is also reported in Table 3.

Total mass concentration of Ag in the standards was measured by ICP-MS *previa* dissolution in HNO₃ 5% v/v and subsequent dilution in NH₄OH 2.8 % w/w. The analysis was carried out in full-quant mode by external calibration with Rh as internal standard.

Methods for μ XRF and μ XANES analyses

Standards and samples

Solid-state reference compounds for μ XANES included: Ag⁰ foil, AgCl, Ag₂SO₄, AgNO₃, Ag₂O, Ag sulfadiazine (AgSD) and a fragment of intact dressing Acticoat Flex3TM. Reference standards of Ag⁰NPs 10 and 100 nm were prepared from mother water suspensions (citrate stabilized, 20 μ g mL⁻¹ as Ag) by deposition of a 20 μ L drop between Ultralene[®] windows and microscopy slides, followed by rapid freezing and freeze-drying for 24 h. A standard of Ag bonded to GSH was prepared by incubating ionic Ag (from AgNO₃, 10 μ g mL⁻¹ as Ag) in a water solution of GSH \sim 0.5 mg mL⁻¹, at 37° C under gentle shaking for 2 h and in dark conditions, followed by freeze-drying as reported above. Standards of Ag⁰NPs 10 nm, ionic Ag and the intact dressing Acticoat Flex3TM (2.45 mg fragment) were also incubated in a water solution containing HSA, (\sim 0.5 mg mL⁻¹) and in whole human plasma, freeze-dried as reported above, and analyzed as unknown samples.

Instrumental parameters and data elaboration

The μ XRF and Ag L_{III}-edge μ XANES measurements were performed using the scanning X-ray microscope of beamline ID21 at the European Synchrotron Radiation Facility (ESRF, Grenoble, France), working at room temperature conditions. Detectors included a Si₃N₇ diode for I₀ and an 80 mm active area Silicon Drift Detector (Bruker) for the emitted fluorescence. Focusing was achieved using fixed curvature Kirkpatrick-Baez mirror optics. The photon flux was 3.6 x 10⁹ ph s⁻¹ at 3.42 keV with a beam size of 1.0 x 1.2 μ m².

μ XRF maps of signal intensities for individual elements (Ag, S and Cl) were collected for preliminary analysis to select optimal regions for the subsequent μ XANES analysis. The μ XRF maps were acquired with variable lateral resolution (0.5 to 2 μ m) and integration time of 100 ms. The raw data (counts) were elaborated using the PyMca software as follows: i) correction for the settling time and conversion to counts per second (cps); ii) deconvolution (batch fitting of the μ XRF spectra); iii) normalization for the incident beam flux.

Batch Ag L_{III}-edge μ XANES spectra of 30 s were collected and averaged for each spot of interest from 3.32 to 3.42 keV energy range with 0.5 eV steps. The beam position was slightly moved from one spectrum to another to avoid radiation damage. At least 10 spectra were averaged for each region of interest. After background removal and normalization, the spectra were calibrated by taking the first inflection point of at 3.3545 keV and then smoothed by interpolation with 5 iterations. The μ XANES spectra of Acticoat Flex3TM and HSA/plasma incubated standards were treated by LCF using the Athena Software with the following set of reference spectra as independent variables: Ag⁰ foil, Ag⁰NPs 10 nm, AgCl, Ag₂SO₄, AgNO₂, Ag₂O, AgSD and AgGSH. A linear term was allowed to compensate for small differences in data normalization, no energy shift was allowed, and weights and their sum were forced to sum to 1. The energy range used for fitting was 3.3345 to 3.4145 keV (e0 - 0.02 to e0 + 0.06). The quality of fitting was quantified by the normalized sum-square residuals $NSS = \Sigma(\mu_{\text{experimental}} - \mu_{\text{fit}})^2 / \Sigma(\mu_{\text{experimental}})^2 \times 100$, where μ is the normalized absorbance. Linear combinations of one, two and three reference standards were examined. The best fit with n+1 components was retained if NSS was decreased by more than 15 % as compared to the best fit using n components. Based on the results, four main Ag species were revealed in the samples: Ag⁰ foil, Ag⁰NPs 10 nm, AgCl and AgGSH; the other minority species were pooled as "other". When two or more fits of equivalent quality (relative difference of

1
2
3 NSS < 10 %) were obtained with different combinations of such a minority species, proportions
4 and NSS were expressed as mean percentage with standard deviation (SD) between brackets,
5 calculated for the equivalent fits.
6

7 The μ XANES spectra acquired in fluorescence mapping mode by scanning the beam with a 2 x 2
8 μm^2 step size and a 50 ms dwell time per pixel with 3 eV energy steps in the region from 3.320 KeV
9 to 3.341 KeV, 0.5 eV from 3.341 KeV to 3.381 KeV, and 1 eV from 3.382 KeV to 3.42 KeV. This
10 resulted in a total of 126 images recorded using a region of interest selective for Ag L3M4 and
11 L3M5 emission lines, corrected for detector dead time (always kept below 20%) and normalized by
12 the incident beam flux. The stack of images was converted to an hdf5 file containing intensities
13 and the energy values for each map to be processed using PyMca for μ XANES spectra extraction.
14 The map was treated by moving merge of the spectra on 2 x 2 pixels areas and with 1 pixel step, in
15 order to reduce the noise and improve the statistical representativity. After background removal
16 and normalization, the spectra were calibrated and individually processed by LCF as above, but
17 using only the reference spectra of Ag⁰NPs 10 nm, AgCl, and AgGSH as independent variables.
18 Based on visual inspection of the fits, an arbitrary threshold of NSS < 0.1 was adopted to remove
19 from the map the pixels with insufficient quality of the fit. A number of pixels in the upper right
20 side of the map (see Fig. 4b) were discarded based on this criterion. These pixels were affected by
21 the sharp change in intensity at the border of the analyzed particle coupled to beam drift caused
22 by scanning the energy with the double crystal monochromator. The retained pixels were re-
23 processed by LCF testing all combinations in which one of the three reference standard was
24 removed. Each standard was considered significant if its introduction decreased the NSS by more
25 than 3 %. This threshold was calibrated *a posteriori* to guarantee that all pixels in the map had at
26 least one significant component, and a coefficient equal to zero was assigned to the non
27 significant components. For each pixel, the coefficients were finally multiplied for the
28 corresponding signal intensity of total Ag (from the μ XRF map), also treated by the moving merge
29 procedure, to obtain the absolute contribute of each species expressed in cps.
30
31
32
33
34
35
36
37
38
39
40
41
42
43
44
45
46
47
48
49
50
51
52
53
54
55
56
57
58
59
60

References

1. Rigo C, Ferroni L, Tocco I, Roman M, Munivrana I, Gardin C, Cairns WRL, Vindigni V, Azzena B, Barbante C, Zavan B (2013) Active Silver Nanoparticles for Wound Healing. *Int J Mol Sci* 14 (3):4817-4840.
2. Wilkinson LJ, White RJ, Chipman JK (2011) Silver and nanoparticles of silver in wound dressings: a review of efficacy and safety. *J Wound Care* 20 (11):543-549.
3. Liu J, Wang Z, Liu FD, Kane AB, Hurt RH (2012) Chemical Transformations of Nanosilver in Biological Environments. *ACS Nano* 6 (11):9887-9899.
4. Reidy B, Haase A, Luch A, Dawson KA, Lynch I (2013) Mechanisms of Silver Nanoparticle Release, Transformation and Toxicity: A Critical Review of Current Knowledge and Recommendations for Future Studies and Applications. *Materials* 6 (6):2295-2350.
5. Gnanadhas DP, Ben Thomas M, Thomas R, Raichur AM, Chakravorty D (2013) Interaction of Silver Nanoparticles with Serum Proteins Affects Their Antimicrobial Activity In Vivo. *Antimicrob Agents Chemother* 57 (10):4945-4955.
6. Liu J, Sonshine DA, Shervani S, Hurt RH (2010) Controlled Release of Biologically Active Silver from Nanosilver Surfaces. *ACS Nano* 4 (11):6903-6913.
7. You CG, Han CM, Wang XG, Zheng YR, Li QY, Hu XL, Sun HF (2012) The progress of silver nanoparticles in the antibacterial mechanism, clinical application and cytotoxicity. *Mol Biol Rep* 39 (9):9193-9201.
8. Pyrz WD, Buttrey DJ (2008) Particle Size Determination Using TEM: A Discussion of Image Acquisition and Analysis for the Novice Microscopist. *Langmuir* 24 (20):11350-11360.
9. Luo P, Morrison I, Dudkiewicz A, Tiede K, Boyes E, O'Toole P, Park S, Boxall AB (2013) Visualization and characterization of engineered nanoparticles in complex environmental and food matrices using atmospheric scanning electron microscopy. *J Microsc* 250 (1):32-41.
10. Grobelny J, DelRio F, Pradeep N, Kim D-I, Hackley V, Cook R (2011) Size Measurement of Nanoparticles Using Atomic Force Microscopy. In: McNeil SE (ed) *Characterization of Nanoparticles Intended for Drug Delivery*, vol 697. *Methods in Molecular Biology*. Humana Press, pp 71-82. doi:10.1007/978-1-60327-198-1_7
11. Hagendorfer H, Kaegi R, Parlinska M, Sinnet B, Ludwig C, Ulrich A (2012) Characterization of Silver Nanoparticle Products Using Asymmetric Flow Field Flow Fractionation with a Multidetector Approach – a Comparison to Transmission Electron Microscopy and Batch Dynamic Light Scattering. *Anal Chem* 84 (6):2678-2685.
12. Proulx K, Wilkinson KJ (2014) Separation, detection and characterisation of engineered nanoparticles in natural waters using hydrodynamic chromatography and multi-method detection (light scattering, analytical ultracentrifugation and single particle ICP-MS). *Environ Chem* 11 (4):392-401.
13. Mitrano DM, Barber A, Bednar A, Westerhoff P, Higgins CP, Ranville JF (2012) Silver nanoparticle characterization using single particle ICP-MS (SP-ICP-MS) and asymmetrical flow field flow fractionation ICP-MS (AF4-ICP-MS). *J Anal At Spectrom* 27 (7):1131-1142.
14. Wimuktiwan P, Shioatana J, Siripinyanond A (2015) Investigation of silver nanoparticles and plasma protein association using flow field-flow fractionation coupled with inductively coupled plasma mass spectrometry (FIFFF-ICP-MS). *J Anal At Spectrom* 30 (1):245-253.
15. Ramos K, Ramos L, Camara C, Gomez-Gomez MM (2014) Characterization and quantification of silver nanoparticles in nutraceuticals and beverages by asymmetric flow field flow fractionation coupled with inductively coupled plasma mass spectrometry. *J Chromatogr* 1371:227-236.

16. Philippe A, Gangloff M, Rakcheev D, Schaumann GE (2014) Evaluation of hydrodynamic chromatography coupled with inductively coupled plasma mass spectrometry detector for analysis of colloids in environmental media - effects of colloid composition, coating and shape. *Analytical Methods* 6 (21):8722-8728.
17. Lewis DJ (2015) Hydrodynamic chromatography - inductively coupled plasma mass spectrometry, with post-column injection capability for simultaneous determination of nanoparticle size, mass concentration and particle number concentration (HDC-PCi-ICP-MS). *Analyst* 140 (5):1624-1628.
18. Soto-Alvaredo J, Montes-Bayon M, Bettmer J (2013) Speciation of Silver Nanoparticles and Silver(I) by Reversed-Phase Liquid Chromatography Coupled to ICPMS. *Anal Chem* 85 (3):1316-1321.
19. Franze B, Engelhard C (2014) Fast Separation, Characterization, and Speciation of Gold and Silver Nanoparticles and Their Ionic Counterparts with Micellar Electrokinetic Chromatography Coupled to ICP-MS. *Anal Chem* 86 (12):5713-5720.
20. Laborda F, Bolea E, Jimenez-Lamana J (2014) Single Particle Inductively Coupled Plasma Mass Spectrometry: A Powerful Tool for Nanoanalysis. *Anal Chem* 86 (5):2270-2278.
21. Yang Y, Long CL, Yang ZG, Li HP, Wang Q (2014) Characterization and Determination of Silver Nanoparticle Using Single Particle-Inductively Coupled Plasma-Mass Spectrometry. *Chin J Anal Chem* 42 (11):1553-1559.
22. Lee S, Bi XY, Reed RB, Ranville JF, Herckes P, Westerhoff P (2014) Nanoparticle Size Detection Limits by Single Particle ICP-MS for 40 Elements. *Environ Sci Technol* 48 (17):10291-10300.
23. Mitrano DM, Ranville JF, Bednar A, Kazor K, Hering AS, Higgins CP (2014) Tracking dissolution of silver nanoparticles at environmentally relevant concentrations in laboratory, natural, and processed waters using single particle ICP-MS (spICP-MS). *Environ-Sci Nano* 1 (3):248-259.
24. Furtado LM, Hoque ME, Mitrano DF, Ranville JF, Cheever B, Frost PC, Xenopoulos MA, Hintelmann H, Metcalfe CD (2014) The persistence and transformation of silver nanoparticles in littoral lake mesocosms monitored using various analytical techniques. *Environ Chem* 11 (4):419-430.
25. Mitrano DM, Leshner EK, Bednar A, Monserud J, Higgins CP, Ranville JF (2012) Detecting nanoparticulate silver using single-particle inductively coupled plasma-mass spectrometry. *Environ Toxicol Chem* 31 (1):115-121.
26. Peters RJB, Rivera ZH, van Bommel G, Marvin HJP, Weigel S, Bouwmeester H (2014) Development and validation of single particle ICP-MS for sizing and quantitative determination of nano-silver in chicken meat. *Anal Bioanal Chem* 406 (16):3875-3885.
27. Loeschner K, Navratilova J, Kobler C, Molhave K, Wagner S, von der Kammer F, Larsen EH (2013) Detection and characterization of silver nanoparticles in chicken meat by asymmetric flow field flow fractionation with detection by conventional or single particle ICP-MS. *Anal Bioanal Chem* 405 (25):8185-8195.
28. Pergantis SA, Jones-Lepp TL, Heithmar EM (2012) Hydrodynamic Chromatography Online with Single Particle-Inductively Coupled Plasma Mass Spectrometry for Ultratrace Detection of Metal-Containing Nanoparticles. *Anal Chem* 84 (15):6454-6462.
29. Grombe R, Allmaier G, Charoud-Got J, Dudkiewicz A, Emteborg H, Hofmann T, Larsen EH, Lehner A, Llinas M, Loeschner K, Molhave K, Peters RJ, Seghers J, Solans C, von der Kammer F, Wagner S, Weigel S, Linsinger TPJ (2015) Feasibility of the development of reference materials for the detection of Ag nanoparticles in food: neat dispersions and spiked chicken meat. *Accredit Qual Assur* 20 (1):3-16.

- 1
- 2
- 3 30. Liu JY, Murphy KE, MacCuspie RI, Winchester MR (2014) Capabilities of Single Particle
- 4 Inductively Coupled Plasma Mass Spectrometry for the Size Measurement of Nanoparticles: A
- 5 Case Study on Gold Nanoparticles. *Anal Chem* 86 (7):3405-3414.
- 6
- 7 31. Cornelis G, Hasselov M (2014) A signal deconvolution method to discriminate smaller
- 8 nanoparticles in single particle ICP-MS. *J Anal At Spectrom* 29 (1):134-144.
- 9
- 10 32. Rigo C, Ferroni L, Tocco I, Roman M, Munivrana I, Gardin C, Cairns W, Vindigni V, Azzena B,
- 11 Barbante C, Zavan B (2013) Active Silver Nanoparticles for Wound Healing. *Int J Mol Sci* 14
- 12 (3):4817-4840.
- 13
- 14 33. Roman M, Rigo C, Munivrana I, Vindigni V, Azzena B, Barbante C, Fenzi F, Guerriero P, Cairns
- 15 WRL (2013) Development and application of methods for the determination of silver in
- 16 polymeric dressings used for the care of burns. *Talanta* 115:94-103.
- 17
- 18 34. Solé VA, Papillon E, Cotte M, Walter P, Susini J (2007) A multiplatform code for the analysis of
- 19 energy-dispersive X-ray fluorescence spectra. *Spectrochim Acta B* 62 (1):63-68.
- 20
- 21 35. Ravel B, Newville M (2005) ATHENA, ARTEMIS, HEPHAESTUS: data analysis for X-ray absorption
- 22 spectroscopy using IFFFIT. *J Synchrotron Radiat* 12 (4):537-541.
- 23
- 24 36. Tuoriniemi J, Cornelis G, Hasselov M (2014) Improving the accuracy of single particle ICPMS
- 25 for measurement of size distributions and number concentrations of nanoparticles by
- 26 determining analyte partitioning during nebulisation. *J Anal At Spectrom* 29 (4):743-752.
- 27
- 28 37. Montano MD, Badiei HR, Bazargan S, Ranville JF (2014) Improvements in the detection and
- 29 characterization of engineered nanoparticles using spICP-MS with microsecond dwell times.
- 30 *Environ-Sci Nano* 1 (4):338-346.
- 31
- 32 38. Hineman A, Stephan C (2014) Effect of dwell time on single particle inductively coupled plasma
- 33 mass spectrometry data acquisition quality. *J Anal At Spectrom* 29 (7):1252-1257.
- 34
- 35 39. Pace HE, Rogers NJ, Jarolimek C, Coleman VA, Higgins CP, Ranville JF (2011) Determining
- 36 Transport Efficiency for the Purpose of Counting and Sizing Nanoparticles via Single Particle
- 37 Inductively Coupled Plasma Mass Spectrometry. *Anal Chem* 83 (24):9361-9369.
- 38
- 39 40. Cedervall T, Lynch I, Lindman S, Berggard T, Thulin E, Nilsson H, Dawson KA, Linse S (2007)
- 40 Understanding the nanoparticle-protein corona using methods to quantify exchange rates and
- 41 affinities of proteins for nanoparticles. *Proc Natl Acad Sci U S A* 104 (7):2050-2055.
- 42
- 43 41. Shannahan JH, Lai XY, Ke PC, Podila R, Brown JM, Witzmann FA (2013) Silver Nanoparticle
- 44 Protein Corona Composition in Cell Culture Media. *PLoS One* 8 (9).
- 45
- 46 42. Rigo C, Roman M, Munivrana I, Vindigni V, Azzena B, Barbante C, Cairns WRL (2012)
- 47 Characterization and evaluation of silver release from four different dressings used in burns
- 48 care. *Burns* 38 (8):1131-1142.
- 49
- 50 43. Adams NWH, Kramer JR (1999) Silver speciation in wastewater effluent, surface waters, and
- 51 pore waters. *Environ Toxicol Chem* 18 (12):2667-2673.
- 52
- 53 44. Larese FF, D'Agostin F, Crosera M, Adami G, Renzi N, Bovenzi M, Maina G (2009) Human skin
- 54 penetration of silver nanoparticles through intact and damaged skin. *Toxicology* 255 (1-2):33-
- 55 37.
- 56
- 57 45. Armitage SA, White MA, Wilson HK (1996) The determination of silver in whole blood and its
- 58 application to biological monitoring of occupationally exposed groups. *Ann Occup Hyg* 40
- 59 (3):331-338.
- 60
- 61
- 62 46. Wang XQ, Kempf M, Mott J, Chang HE, Francis R, Liu PY, Cuttle L, Olszowy H, Kravchuk O, Mill J,
- 63 Kimble RM (2009) Silver Absorption on Burns After the Application of Acticoat (TM): Data
- 64 From Pediatric Patients and a Porcine Burn Model. *J Burn Care Res* 30 (2):341-348.
- 65
- 66 47. Schneider L, Korber A, Grabbe S, Dissemmond J (2007) Influence of pH on wound-healing: a new
- 67 perspective for wound-therapy? *Arch Dermatol Res* 298 (9):413-420.

Table 1 Semiquantitative speciation of Ag in the dressing Acticoat Flex3™, 10 nm size AgNPs and ionic Ag incubated in solutions containing HSA or in whole human plasma for 2 h. Data were obtained by LCF of the μ XANES spectra; the AgGSH standard is representative of Ag-thiol bonds.

Experiment	Species	Molar fraction %
Ag ⁰ NPs 10 nm in plasma	Ag ⁰ foil	66
	Ag ⁰ NPs 10nm	28
	other	6
Ag ⁺ in plasma	AgCl	63
	other(x2)	37
Ag ⁰ NPs 10 nm in HSA	Ag ⁰ NPs 10nm	93
	AgGSH	7
Ag ⁺ in HSA	AgGSH	67
	other	33
Acticoat Flex3™	Ag ⁰ NPs 10nm	66
	Ag ⁰ foil	34
Acticoat Flex3™ in plasma	AgCl	59
	Ag ⁰ NPs 10nm	32
	AgGSH	10

Table 2 Main clinical information on the burnt [adult](#) patients treated with Acticoat Flex3™, and concentration of total Ag and dissolved Ag fraction in their whole blood.

	Patient A		Patient B	Patient C
Burn location	Torso + left arm		Torso	Torso + arms
Burned body surface, %	22		27	30
Degree	II		II	II
Dermabrasion	yes		yes	yes
Treatment duration, days	3	6	3	3
Total Ag in blood, ng mL ⁻¹	46.6	48.9	83.1	36.9
Total Ag in centrifugated blood, ng mL ⁻¹ (recovery %)	44.5 (96)	46.7 (96)	81.4 (98)	28.1 (76)
Dilution factor	100	100	250	75
Dissolved Ag in centrifugated blood, ng mL ⁻¹ (molar fraction %)	37.9 (85)	41.6 (89)	83.9 (103)	28.0 (100)

For Peer Review

Table 3 Characterization of the AgNPs standards (mother suspensions) used throughout the study. Particles' diameter and geometry were measured by TEM on a minimum sample of 400 particles; for the z-potential $n = 5$.

Nominal size \pm SD (nm)	Measured diameter (nm):		Geometry:		z-potential (mV)
	Median (interquartile range)	Average \pm SD	Circularity \pm SD	Roundness \pm SD	
	Mode		Solidity \pm SD		
10 ± 4	8.6 (7.1 – 10.8)		0.90 ± 0.03		-46.4 ± 2.2
	9.2 ± 3.2		0.91 ± 0.06		
	7.2		0.95 ± 0.01		
20 ± 4	22.2 (20.7 – 23.5)		0.90 ± 0.02		-46.6 ± 2.0
	21.9 ± 2.4		0.91 ± 0.05		
	23.1		0.95 ± 0.01		
40 ± 4	40.7 (40.2 – 45.1)		0.89 ± 0.02		-45.3 ± 1.7
	42.4 ± 3.8		0.90 ± 0.05		
	43.5		0.96 ± 0.01		
60 ± 4	56.4 (50.6 – 59.7)		0.89 ± 0.02		-48.6 ± 1.2
	56.5 ± 4.5		0.89 ± 0.06		
	58.7		0.96 ± 0.01		
100 ± 4	98.7 (95.6 – 102.3)		0.88 ± 0.02		-53.2 ± 1.4
	99.0 ± 5.1		0.89 ± 0.05		
	98.7		0.95 ± 0.01		

Figure captions

Fig. 1 External calibrations applied to elaborate the HDC-spICP-MS chromatograms. a) 1st-99th interpercentile range of the normalized signal intensity relative to the average value calculated for dissolved Ag 500 pg mL⁻¹ within 2 s time windows, plotted against the corresponding average intensity. The range was adopted as the variable threshold for deconvolution of dissolved Ag and AgNPs signals. b) Calibration of the normalized signal intensity as a function of the mass of AgNPs standards with 20, 40, 60 and 100 nm nominal diameter (hypothesis of purely metallic spherical particles, n = 3). c) Calibration of the elution time as function of the diameter of AgNPs standards with 20, 40, 60 and 100 nm nominal diameter (n = 3). d) Calculation of the AgNPs detection efficiency as slope of the regression line, detected mass vs. injected mass (bilog scale). The injected standards were: 20 nm (5, 10, 20, 30, 40 pg), 40 nm (2.5, 5, 10, 20, 50 pg), 60 nm (10, 20, 50, 100, 200 pg) and 100 nm (25, 50, 100, 200, 500 pg). e) Calibration of the peak area for dissolved Ag (n = 3).

Fig. 2 3D contour plot chromatograms of AgNPs obtained for a mixture of 20, 40, 60 and 100 nm standards diluted in mobile phase (a, b) and the same mixture incubated for 2 h in plasma (c, d).

Fig. 3 a) Temporal variation of the molar fractions of AgNPs and dissolved Ag in plasma after incubation of a 100 nm standard from 2 to 24 h, average \pm standard deviation, n = 3. b) Temporal variation of the mode of the AgNPs mass-derived distribution in the same incubated standard, average \pm theoretical uncertainty, n = 3.

Fig. 4 3D contour plot chromatograms of AgNPs after incubation of the dressing Acticoat Flex3TM in plasma for 2 h.

Fig. 5 a) μ XANES spectra of pure standards of Ag species; b) μ XANES spectra of the intact dressing Acticoat Flex3TM, and AgNPs 10 nm and ionic Ag incubated in a solution containing HSA or in whole human plasma. The original spectra of the incubated standards are superimposed to their best fitting (dotted lines) obtained by LCF using the pure standards as the input variables. The fitting parameters (molar fractions) are reported in Table 1. AgGSH is representative of the Ag-thiol bounds.

Fig. 6 a) μ XRF map of the distribution of Ag, Cl and S in the region surrounding a micrometric agglomerate of AgNPs released by Acticoat Flex3TM after 2 h incubation in plasma. Scale is linear in cps with independent full-scale values. b) μ XANES map of Ag speciation in the same region. Scale is linear in cps with the same full-scale value for all species. AgGSH is representative of the Ag-thiol bounds.

Fig. 7 Deconvoluted chromatograms of dissolved Ag in whole blood of burnt patients obtained by HDC-spICP-MS. The blood was collected 3 days (patients A3, B and C) and 6 days (patient A6) after the application of the dressing Acticoat Flex3TM containing AgNPs. Each sample was differently diluted (see Table S-1) before injection to achieve a comparable concentration (\sim 400 pg mL⁻¹).

Fig. 8 TEM images of the AgNPs standards (mother suspensions) used throughout the study; the nominal sizes are 10 (a), 20 (b), 40 (c), 60 (d) and 100 (e) nm

Online Abstract Figure Simplified scheme of the combined analytical approach adopted for studying the chemical dynamics of AgNPs in human plasma/blood.

For Peer Review

1
2
3
4
5
6
7
8
9
10
11
12
13
14
15
16
17
18
19
20
21
22
23
24
25
26
27
28
29
30
31
32
33
34
35
36
37
38
39
40
41
42
43
44
45
46
47
48
49
50
51
52
53
54
55
56
57
58
59
60

Prof. Alfredo Sanz-Medel

Editor,

Dr. Nicola Oberbeckmann-Winter

Managing Editor,

Analytical and Bioanalytical Chemistry

Venice, 20 August 2015

Reference: Manuscript ID: ABC-01228-2015

Dear Editors,

I enclose the revised version of our paper entitled: "Hydrodynamic chromatography coupled to single-particle ICP-MS for the simultaneous characterization of AgNPs and determination of dissolved Ag in human plasma and blood of burnt patients"

by Marco Roman, Chiara Rigo, Hiram Castillo-Michel, Ivan Munivrana, Vincenzo Vindigni, Ivan Mičetić, Federico Benetti, Laura Manodori and Warren R.L. Cairns.

We appreciate the positive judgment given by the Editor and the Referees to our work. We have carefully considered their comments when preparing this revised version of improved quality. A detailed list of the responses to the points raised during the evaluation of the manuscript is provided below, and is traced in the amended version of the revised manuscript. A new figure and corresponding caption is also provided to be used as accompanying graphic for the online abstract.

Editor

The authors have made important contributions here with respect to the use of HDC coupled to ICP-MS in single particle mode (deconvolution of dissolved and NP signals, determination of dissolved silver), applying this methodology to complex samples for the first time.

Thus, I agree with both referees that the MS deserves publication in ABC.

We thank the Editor for appreciating the impact and the quality of our study concerning both the analytical aspects and the applicative implications.

However, both expert reviewers have raised some minor points to enhance the quality of the final MS. In particular, the overall novelty here is not highlighted enough (see referee 2 comments) and should be better detailed in the revised version.

We agree with the Editor and Referee B in considering the need to highlight the analytical novelty beside the specific medical application. Accordingly with the detailed comments of Referee B (see below), we made the following changes to give more emphasis to the innovative methodological aspects:

- 1) The title was changed in: "Hydrodynamic chromatography coupled to single-particle ICP-MS for the simultaneous characterization of AgNPs and determination of dissolved Ag in human plasma and blood of burnt patients"
- 2) The abstract was substantially modified to be focused on the analytical method.
- 3) The conclusion was significantly expanded (doubled) starting from page 11 line 23, to highlight the methodological novelties and their potential impact for the scientific community.

Referee A

Generally a very detailed and clear manuscript that shows the application of a hyphenated technique with spICP-MS data acquisition. This combination clearly complements the strengths and weaknesses of both techniques.

We thank the Referee for appreciating the technical quality of our work.

There are a few points where additional comments by the author would be helpful:

- *Why was the instrument tuned with respect to oxide formation using Ce? For spIC-MS, detection sensitivity is decisive, and hence a dedicated Tuning for the element that is actually targeted may lead to improved particle size detection limits. This was correctly accomplished through tuning using a 1 ng mL solution of Ag, but in my opinion the sensitivity could be further improved if oxide Formation below 2% would have been discarded as a tuning criterion.*

Choosing between tuning for sensitivity and tuning for robustness (as measures by the Ce oxide ratio) is an interesting point in spICP-MS. It is true that tuning for sensitivity would have a direct advantage in lowering the minimum detectable particle size and dissolved Ag concentration. However, in our study we also engaged the challenge of applying sp to heavy matrices: not only the plasma and whole blood, but also the mobile phase (included with a high flow rate). In this case signal suppression or just fluctuation due to matrix effects, and background rising after repeated injections could seriously affect the overall reliability of the method, thus we preferred to adopt robust plasma conditions. For the same reason, for example, we kept the sample depth at 8 mm. We mentioned the motivation of our choice in this revised version of the manuscript at page 4 line 38.

- *The term limit of detection in conjunction with spICP-MS needs additional clarification since it can be understood in two ways: The lowest detectable particle size and the lowest detectable particle number. Whereas the first one describes an Instrument related characteristic, the latter one represents a statistical consideration of the number of evaluated signals. Experts in the field are able to distinguish the correct use, but people not directly familiar with the technique may be confused.*

A third definition of the LOD is also used in this paper, which is the lowest detectable concentration of dissolved Ag. We agree that the manuscript in its original form was not sufficiently clear for a generic reader, thus we made the following changes:

- 1) A short definition of the three LODs is given at the beginning of the discussion section (par. 2.1.1. page 5 line 12) and specific acronyms are introduced to be used along the whole manuscript.
- 2) An estimation of the LOD for the number of particles, originally missing, is now provided and briefly discussed at page 7 line 5.

- *Has the number of wound dressings that all patients received been identical? With what frequency is the dressing exchanged? This information is relevant to judge the exposure to ionic silver over the entire Treatment, and would definitely influence the concentration of Ag in whole blood over time.*

The referee is absolutely right, these points are pivotal. At page 10 line 10 we mention now that all patients were treated with a single application of the dressing. Concerning the number of dressings,

1
2
3 that's a more complex issue: application is the last step of a surgical intervention in which the
4 dressing is cut out and modeled depending on the specific shape and characteristics of the wound.
5 Thus, referring to the number of dressings would be not so informative, while the % of burned body
6 surface (reported in Table 2), which is entirely treated, is a good estimate of the wound area
7 exposed to Ag. We now mention also this at page 10 line 10.
8

9
10 - Page 3, line 3: should be recent introduction of THE single-particle ...

11
12 The sentence was changed accordingly.

13
14 - The reference "Table 1" on page 10 is not correct. The clinical Information is displayed in table 2.

15
16 The referee is right, the number was changed accordingly.
17

18 Referee B

19
20 *The work has enough significance, originality, interest and quality to deserve publication.*

21
22 We thank the Referee for appreciating the novelty and quality of our work.
23

24
25 *However, the manuscript is unbalanced in the sense that the title, the abstract and the main*
26 *conclusions are related to the study about the fate of silver NP and silver NP-coated dressing in*
27 *human plasma by HDC-sp-ICPMS and μ XRF and μ XANES, as well as the fate of silver NP-coated*
28 *dressing after topical administration in burnt patients. On the other hand, the authors have made*
29 *novel contributions with respect to the use of HDC coupled to ICP-MS in single particle mode*
30 *(deconvolution of dissolved and NP signals, determination of dissolved silver), applying this*
31 *methodology to complex samples for the first time. In my opinion, this methodological part is not*
32 *highlighted enough. At least, the title and the abstract should reflect these novelties.*
33

34
35 We agree with this comment, which was also supported by the Editor, and made the changes
36 reported above.
37

38 Additional comments

39
40 *The authors mention a "detection efficiency" (p.6 l. 41, p.8 l.14) as a corrected transport efficiency*
41 *(in fact, nebulization efficiency) taking into account the settle time. In my opinion, this correction is*
42 *unnecessary, if all data acquisition is performed under the same conditions. Moreover, this*
43 *detection efficiency is not considered in equation 1 or any other calculation shown.*
44

45
46 This issue was probably presented in a bad way in the original version of the manuscript.
47 Differently by all works on spICP-MS in the literature, we acquired 2 masses. This introduced a
48 settling time, which affects the number of detected particles beside the classical transport
49 (nebulization) efficiency. The referee is right: since the efficiency is calibrated under the same
50 conditions, correcting for the settling time is irrelevant for the final results. However, introducing
51 the correction allows providing a value for transport efficiency which is more correct with respect
52 to its definition, and directly comparable with the literature.

53
54 For this reason, in this revised version we preferred keeping the settling time correction, but we
55 made some changes in order to make the text more simple and clear (without any change in the
56 meaning of the contents):

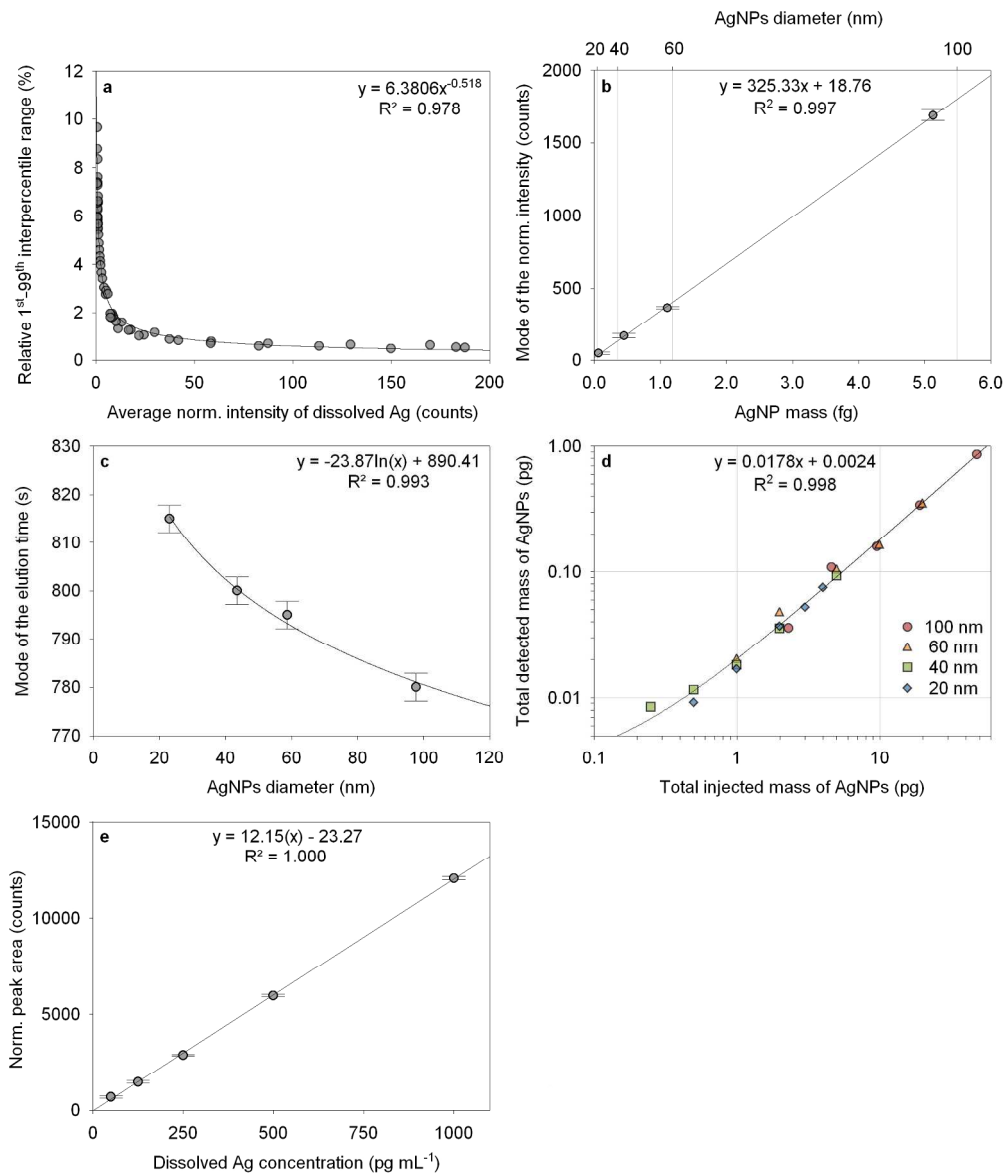
57
58 1) At page 5 line 38, explaining the choice of the acquisition strategy, we added the sentence "In
59 addition, the acquisition of two masses introduces a settling time, which slightly affects the
60 number of detected particles (see section 2.1.4)." to make explicit the origin of the correction.

1
2
3 2) In the paragraph 2.1.4. we removed the confusing concept of “detection efficiency”. The settling
4 time correction was explicated in eq. 1 to make possible referring directly to the transport
5 efficiency along the rest of the manuscript.
6

7 *The nebulization efficiency calculated (p. 7 l.5-8) is characteristic of the nebulizer, spray chamber*
8 *and flow rate used. Thus there is no point to compare the nebulization efficiency obtained by the*
9 *authors with the Pergantis' values that was obtained with a different nebulization system. Please*
10 *remove the comments.*
11

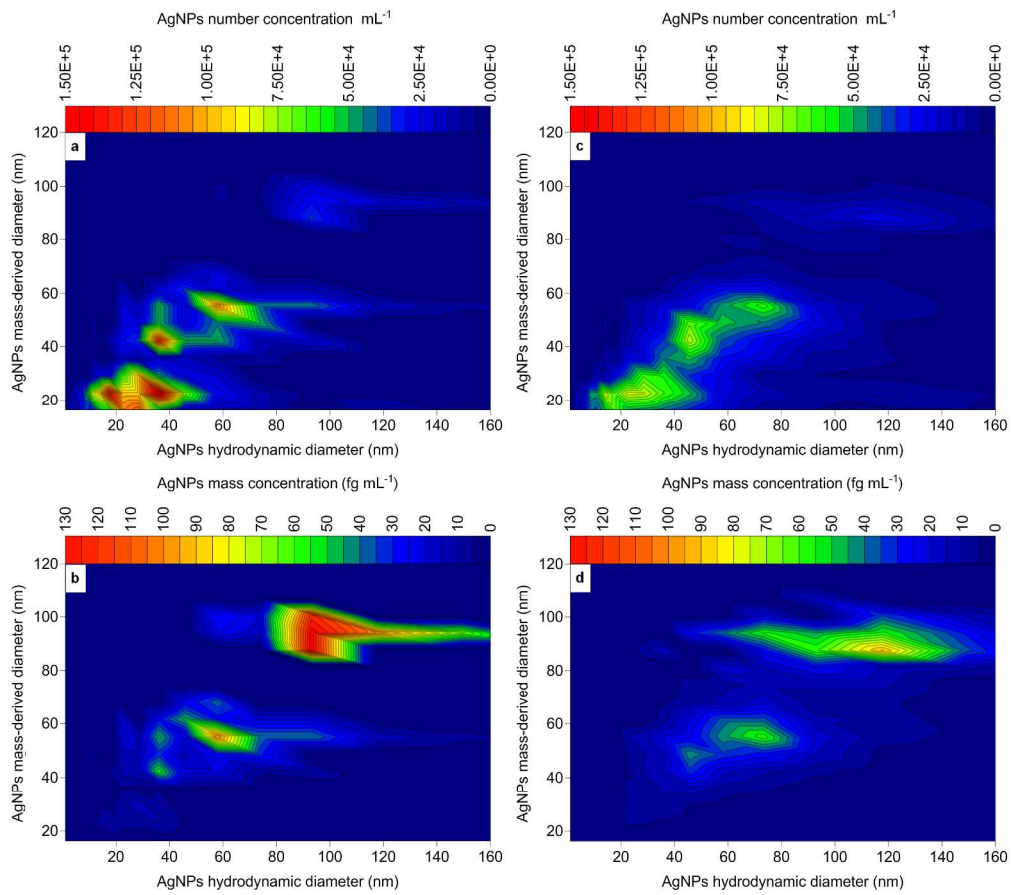
12 The sentence was removed.
13
14
15
16
17
18
19
20
21
22
23
24
25
26
27
28
29
30
31
32
33
34
35
36
37
38
39
40
41
42
43
44
45
46
47
48
49
50
51
52
53
54
55
56
57
58
59
60

For Peer Review



623x733mm (96 x 96 DPI)

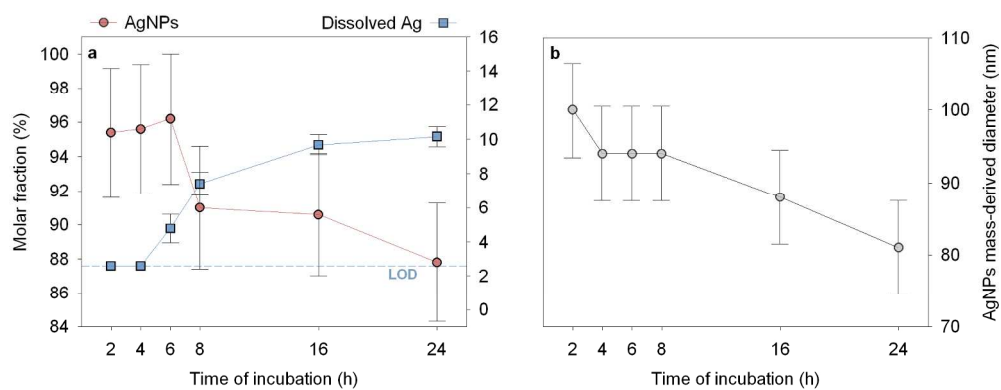
1
2
3
4
5
6
7
8
9
10
11
12
13
14
15
16
17
18
19
20
21
22
23
24
25
26
27
28
29
30
31
32
33
34
35
36
37
38
39
40
41
42
43
44
45
46
47
48
49
50
51
52
53
54
55
56
57
58
59
60



235x206mm (300 x 300 DPI)

iew

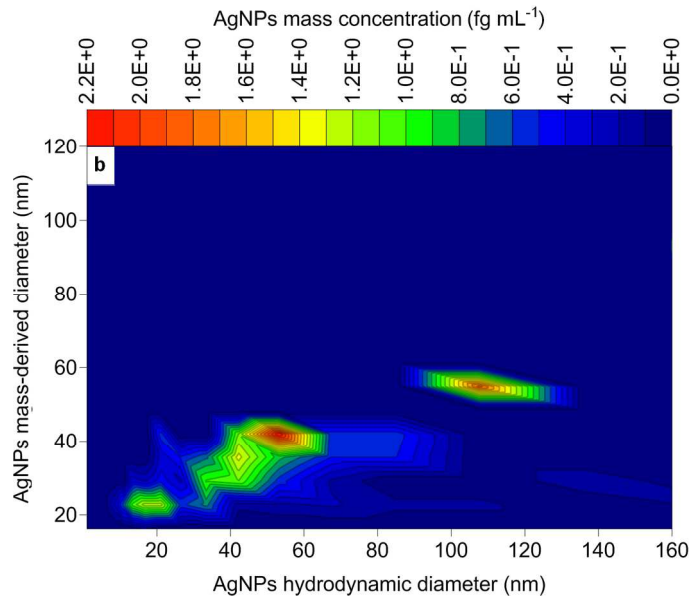
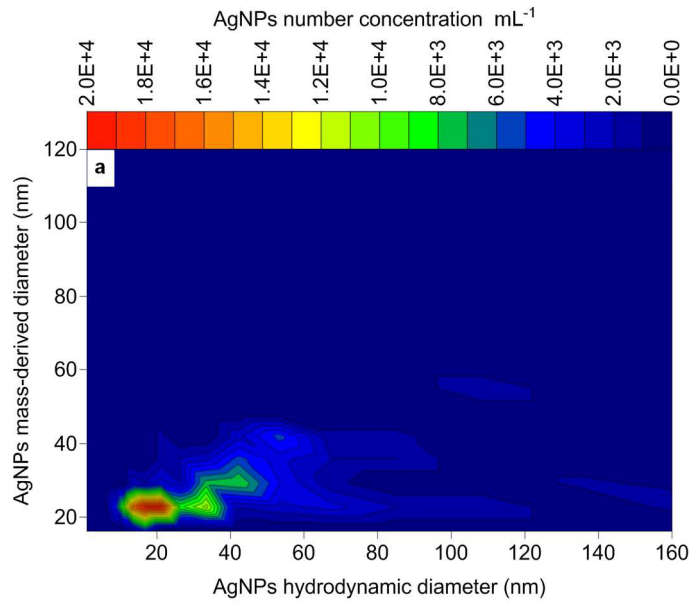
1
2
3
4
5
6
7
8
9
10
11
12
13
14
15
16
17
18
19
20
21
22
23
24
25
26
27
28
29
30
31
32
33
34
35
36
37
38
39
40
41
42
43
44
45
46
47
48
49
50
51
52
53
54
55
56
57
58
59
60



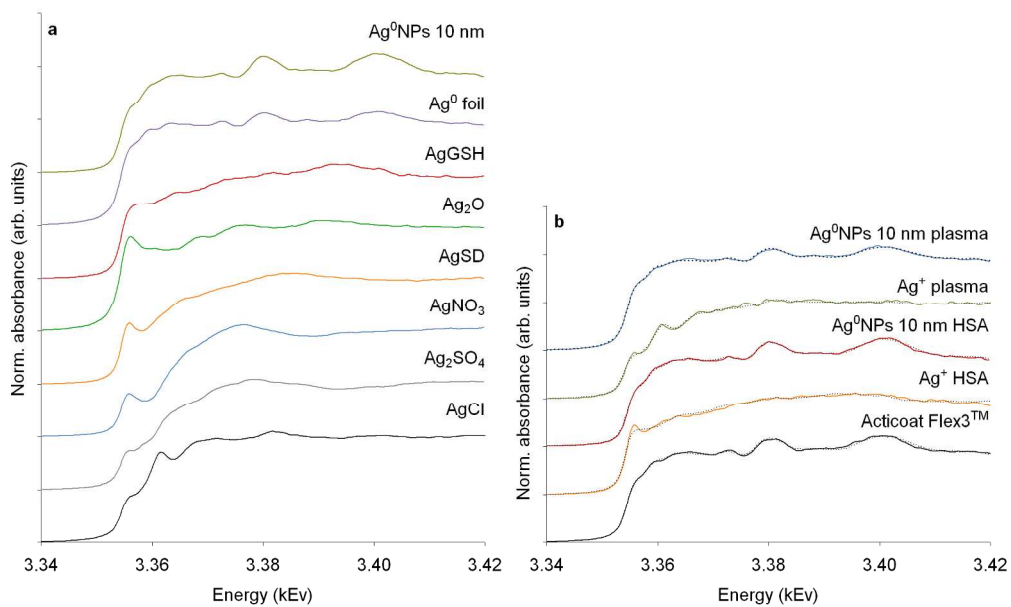
623x249mm (96 x 96 DPI)

Peer Review

1
2
3
4
5
6
7
8
9
10
11
12
13
14
15
16
17
18
19
20
21
22
23
24
25
26
27
28
29
30
31
32
33
34
35
36
37
38
39
40
41
42
43
44
45
46
47
48
49
50
51
52
53
54
55
56
57
58
59
60



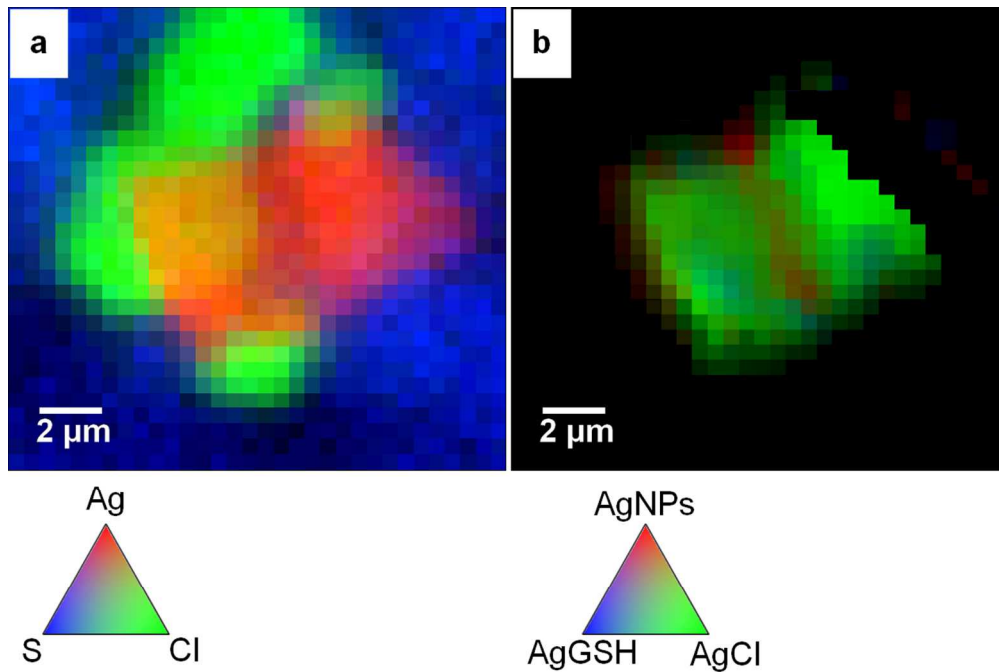
115x204mm (300 x 300 DPI)



617x370mm (96 x 96 DPI)

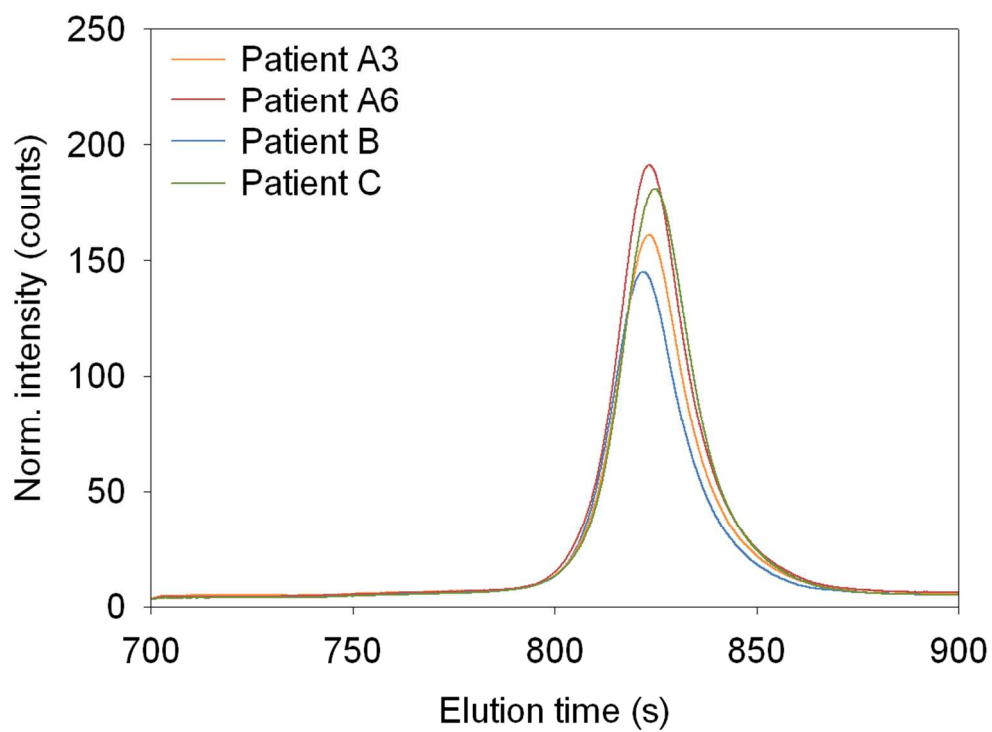
Review

1
2
3
4
5
6
7
8
9
10
11
12
13
14
15
16
17
18
19
20
21
22
23
24
25
26
27
28
29
30
31
32
33
34
35
36
37
38
39
40
41
42
43
44
45
46
47
48
49
50
51
52
53
54
55
56
57
58
59
60



334x225mm (96 x 96 DPI)

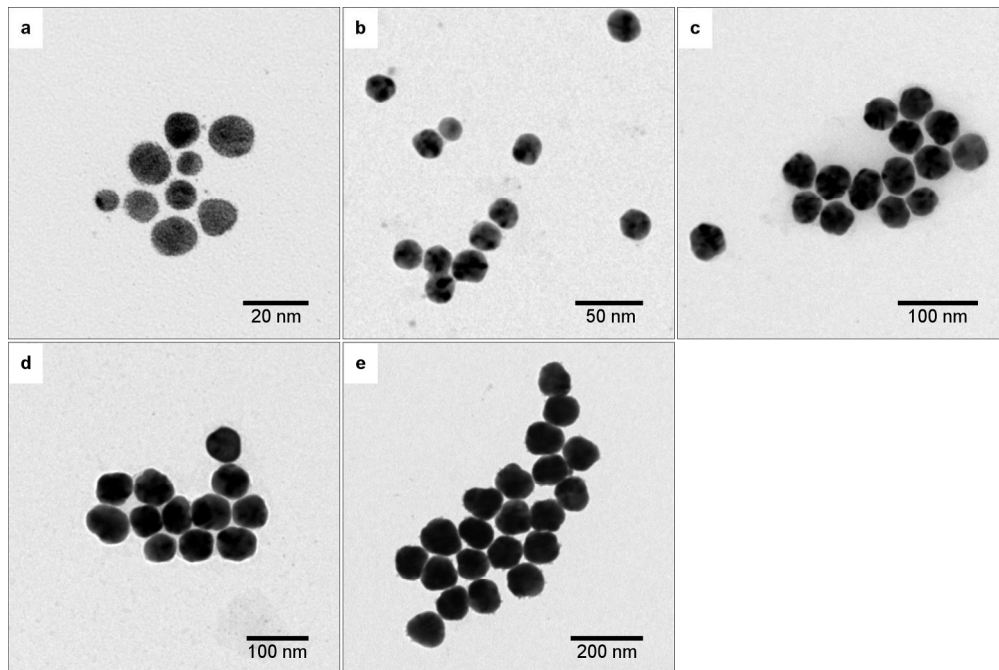
Review



311x233mm (96 x 96 DPI)

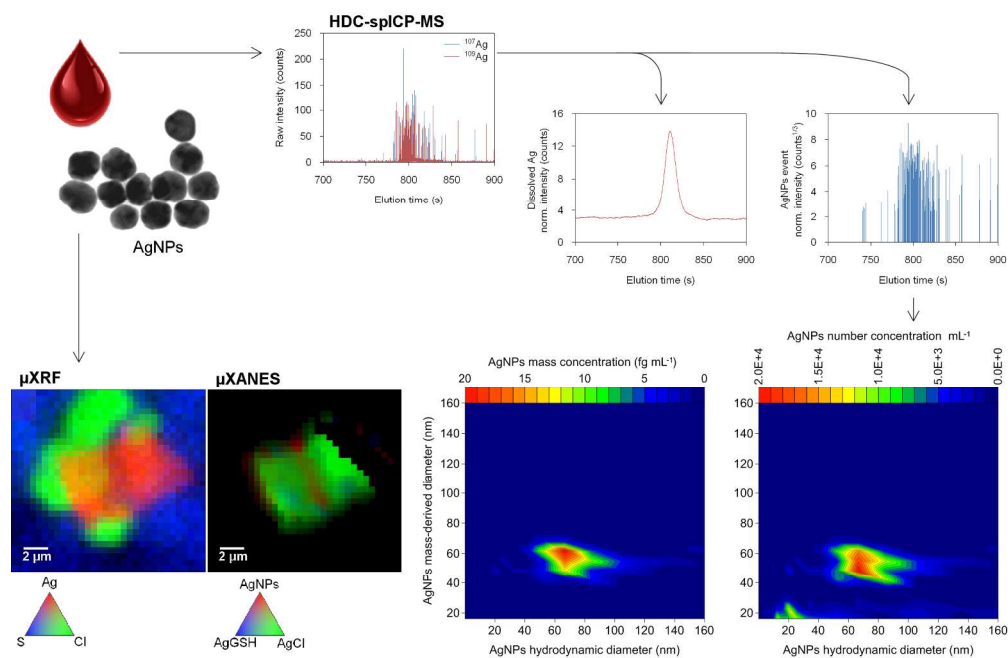
review

1
2
3
4
5
6
7
8
9
10
11
12
13
14
15
16
17
18
19
20
21
22
23
24
25
26
27
28
29
30
31
32
33
34
35
36
37
38
39
40
41
42
43
44
45
46
47
48
49
50
51
52
53
54
55
56
57
58
59
60



185x123mm (300 x 300 DPI)

Review



Simplified scheme of the combined analytical approach adopted for studying the chemical dynamics of AgNPs in human plasma/blood
653x427mm (96 x 96 DPI)

Review